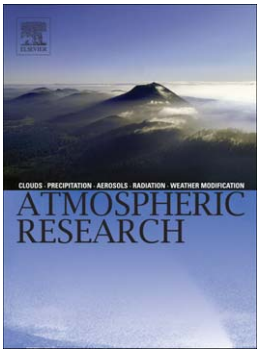

Statistical downscaling and Attribution of air temperature change patterns in the Valencia region (1948-2011)

Juan Javier Miró Pérez, María José Estrela Navarro, Jorge Olcina Cantos

PII: S0169-8095(15)00020-4
DOI: doi: 10.1016/j.atmosres.2015.01.003
Reference: ATMOS 3329

To appear in: *Atmospheric Research*

Received date: 14 October 2014
Revised date: 9 January 2015
Accepted date: 9 January 2015

Please cite this article as: Pérez, Juan Javier Miró, Estrela Navarro, María José, Olcina Cantos, Jorge, Statistical downscaling and Attribution of air temperature change patterns in the Valencia region (1948-2011), *Atmospheric Research* (2015), doi: 10.1016/j.atmosres.2015.01.003

STATISTICAL DOWNSCALING AND ATTRIBUTION OF AIR TEMPERATURE CHANGE PATTERNS IN THE VALENCIA REGION (1948-2011)

Juan Javier Miró Pérez
C/Ancha 21, 03420 Castalla (Alicante), Spain.
castalium@gmail.com
María José Estrela Navarro
Laboratorio de Meteorología-Climatología, Unidad Mixta CEAM-UVEG. Departament de Geografia Física, Universitat de València, Avda. Blasco Ibáñez 28, 46010, Valencia, Spain.
Maria.Jose.Estrela@uv.es
Phone +34 963983129
Jorge Olcina Cantos
Laboratorio de Climatología, Instituto Interuniversitario de Geografía, Universidad de Alicante, Ctra. San Vicente del Raspeig s/n - 03690 San Vicente del Raspeig – Alicante, Spain.
jorge.olcina@ua.es

ABSTRACT
This study is based on the statistical downscaling and spatial interpolation of high-resolution temperatures (90 m) over the 1948-2011 period performed for the Valencia Region (east Iberian Peninsula) after considering local topographical factors in the fine-scale distribution of temperatures. The objective was to detect the areas that were potentially more vulnerable to air temperatures change. This allowed the detection of local climate change patterns, which were analysed and found to be consistent in spatial and temporal terms. These patterns indicate a more marked warming tendency in higher parts of reliefs and their slopes. However, this tendency is less pronounced in bottoms of valleys and on coastal plains, particularly for minimum temperatures, while the tendency for increasing maximum temperatures becomes more generalised. These patterns seem to connect well with regional changes in pressure fields, wind frequency, precipitation patterns and sea surface temperature.

Key words: Temperature, climate change, local patterns, local vulnerability.

1. INTRODUCTION

Based on current knowledge of climate change, the need to study its regional and local processes more accurately is more than evident since this is precisely where most uncertain aspects are found. Availability of long temperature series in the Mediterranean region of the Iberian Peninsula has enabled the determination of general growing air temperature trends for this region by means of relative homogenisation processes (Quereda *et al*., 2000; Miró *et al*., 2006a; Brunet *et al.*, 2007; Quereda *et al*., 2009; Bladé & Castro Díez, 2010; Del Río *et al.*, 2012). However, the spatial density of these long series has not allowed a local scale to be obtained that identifies the fine-scale behaviour of climate change. It is here where statistical downscaling (SD) tools prove useful (Hewitson & Crane, 1996; Wilby *et al*., 1998) as they allow the reconstruction of missing temporal and spatial information from available information and its

extrapolation to future scenarios. This approach is becoming mainstreamed, as evidenced by the CORDEX2 activity of the World Climate Research Programme.

The strong point of SD tools is the possibility of fitting a signal over the real data observed on a local scale, as well as its low computational cost compared to dynamic downscaling. In addition there are controversies regarding the dynamical downscaling ability to adding more information at different scales from general circulation models or reanalysis without local information for reference considered in the SD (Xue *et al.*, 2014) . However, the weak point for SD lies in the stationary relationships on which the obtained local models are based, which could vary with time, specifically by forcings caused by climate change (Wilby *et al*., 2004). Regarding the value of multiple downscaling techniques for the current status, some have been found to be pessimistic (e.g. Pielke and Wilby 2012), but others are more optimistic (e.g. Maraun *et al*. 2010). This entails the recommendation of reaching an SD that is as plausible, defensible and actionable as possible (Hewitson *et al*. 2014). Therefore, the present study focuses on the results of SD dedicated to the reconstruction and filling in of the daily temperature series observed, validated with the observed data and consistent results in spatial and temporal terms. This work commences from that conducted by Miró *et al*. (2012), Miró (2014) and Miró *et al*. (2014), which provide details of how the data employed herein were obtained,:

1. The set of the observed series employed and homogeneity.

2. The SD process followed and its validation. This process enabled the reconstruction of over 300 temperature series in the study area (the Valencia Region) over the 1948-2011 period with homogenity and without gaps. Originally, only three of all the observed series completely covered this period.

3. The spatial interpolation (SI) of the temperaturas obtained from the new density of the available series in the region after SD, along with its validation, which contemplated peaks of mountains with lower station density.

4. Grouping the SD series into clusters according to the ratio between the air temperature change trends noted during the study period and the local physical characteristics of their location (station).

The present study focuses on the Valencia Region and bordering areas (Figure 1). It consists in showing and analysing the results of the SD and spatial interpolation (SI) of daily temperatures, obtained in this region according to Miró *et al*. (2012; 2014) and Miró (2014). The general objective was to analyse air temperature change trends in the study area between 1948 and 2011 according to SD-SI. There were two subsequent specific objectives: to show the most relevant and consistent change patterns on a local scale; to provide further evidence that supports/explains these change patterns.

In the study area, no attempts have been made to date to study air temperature change patterns on a local and finer scale, despite the above-cited studies having done general analyses in the study area. This justifies the novel aspect of the present research, particularly as other inicipient studies in different world areas with similar latitudes, and in regions of complex terrain, are finding distinct local air temperature change patterns, especially through disconnected trends by air temperatures decoupling between valleys and mountains with minimum temperatures (Daly *et al*., 2010; Pepin *et al.*, 2011; Dobrowski *et al.*, 2011). In the study area, different trends for minimum temperatures in nearby locations have already been suggested (Miró, 2014; Miró et al., 2014) in relation to a distinct sensitivity to air temperature inversions caused by increased and more favourable stable situations.

The present study extends the results and connections of this line of work, which is also novel given the Iberian Peninsula and Mediterranean setting.

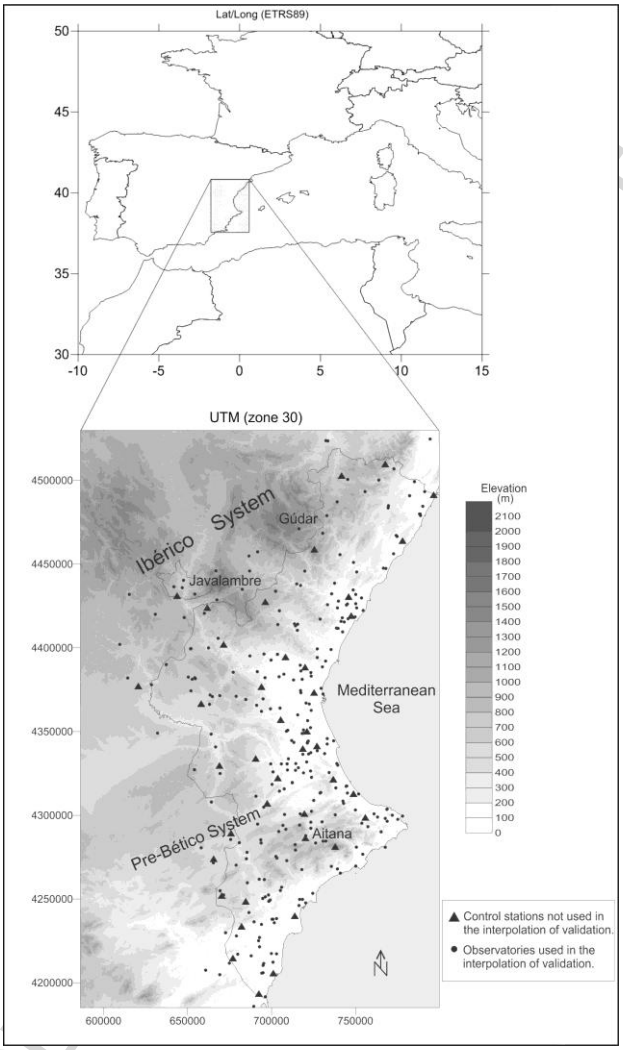

Figure 1: Study area (western Mediterranean Basin) and location of the 40 meteorological stations used for cross-validating spatial interpolation.

2. DATA AND METHODS

The series of air temperature trends, and the maps of the maximum (Tmax), minimum (Tmin) and mean (Tmed) temperatures presented in this paper, derive from the variety of the SD and SI methodological procedures discussed, described in detail and performed in Miró *et al*. (2012; 2014) and Miró (2014). The present study deals with the monthly and yearly results obtained from the cited publications and some climate connections. Nonetheless, essential information about these data and methods is included herein.

2.1. Air temperature data and reconstruction

SD was performed for 314 Tmax series and 320 Tmin series (observed) in the Valencia Region and bordering areas. This refers to the daily series corresponding to automatic and manual stations of official organisation networks or important research institutions in the region:

- AEMET <http://www.aemet.es>
- CEAM <http://www.ceam.es>, <http://www.ceam.es/ceamet>

- SIAR-IVIA <http://www.ivia.es/>, <http://eportal.magrama.gob.es/websiar>
- SIAR (other Spanish Autonomous Communities) <http://eportal.magrama.gob.es/websiar>
- IIG <http://iig.ua.es/>, <http://m.web.ua.es/es/labclima/>

The basic selection criterion was a minimum, continuous 10-year duration covering the 1948-2011 period. However, this criterion was reduced to 8 years for mountainous areas with lower station density (for automatic stations in which SD was particularly good).

Initially, 326 stations were submitted to SD, and 12 Tmax series and 6 Tmin ones were ruled out for providing SD of a significantly poorer quality than the rest. This was due to the poor quality of the specific series observed, while SD obtained good results in neighbouring series in a similar location. In general terms, SD was more accurate for automatic stations than for manual ones as poor quality recordings were found in the latter. Examples of both cases are provided (Figure 2).

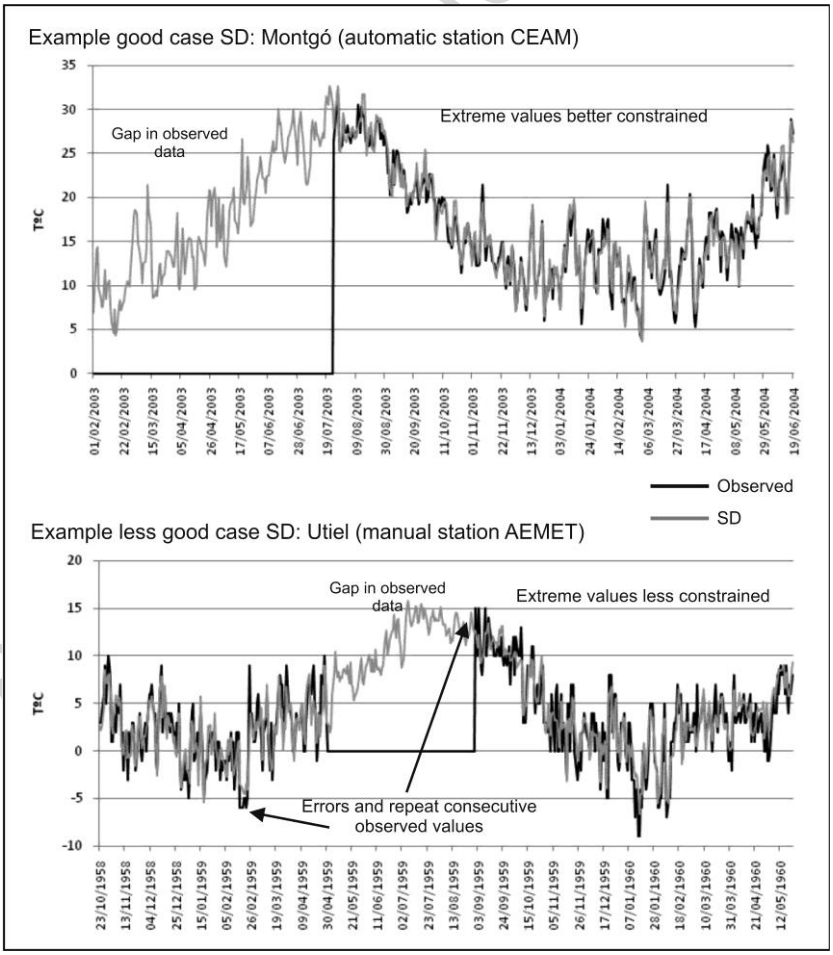

Figure 2: An example of adjusting SD to daily observed data, and to filling in its gaps. Above, an observed quality series. Below, an observed series with no record of decimals, but with suspicious data.

SD was always more accurate between the 25 and 75 percentiles (daily data) and, as expected, extreme values tended to be underestimated (percentiles > 90 and < 10). This implied having to apply a final correction to SD per percentile range to improve estimating daily extreme values. This calculation was done separately per month and particular series to compare their observed daily series (available stretches) with SD

within each percentile range. A sample (averaged case) of the correction made (bias) is offered in Table 1.

TMAX						
Bias Percent. <=5	Bias Percent. <=10	Bias Percent. 10-25	Bias Percent. 25-75	Bias Percent. 75-90	Bias Percent.>= 90	Bias Percent.>= 95
-1.80	-1.45	-0.63	0.01	0.61	1.42	1.81
TMIN						
-2.03	-1.68	-0.81	0.07	0.79	1.34	1.56

Table 1: Average negative bias in ºC that the daily data deriving from SD present compared with the observed data, per percentile range, averaged for all series and months.

The cross-validation of SD was always done on stretches of series not used for training the SD model. However, the best final SD resulted from performing multiple SD on the sectorial stretches of each series. After testing the homogeneity of the available observed series, probable rupture points were delimited, which helped differentiate various streatches in each series. For each stretch, sectorial SD (sSD) was done. Attempts were made to not use stretches with less than 10 years and the object was triple. Firstly, it helped avoid lack of homogeneity in the observed data as it would affect SD performance. To this end, the probable loss of the local components that clashed with the general climate signal was avoided as it could be caused by circular homogenisation methods. Secondly, it helped test the coherence of sSD for each series (sSDs) during the extrapolated period. This allowed us to see if the stationary relationships that sustained SD had been maintained throughout the study period. Thirdly, it allowed the elimination of probable spurious long-term trends in the observed series. This was evident with the Tmin series from the stations that have been most affected by growing peri-urbanisation in the last few decades. This did not apply to more rural stations.

An example of how to configure all sSDs for each series is provided in Figure 3. Table 2 depicts the correlation matrix found between sSDs by taking the averaged case of all the series with four stretches or more of the available sSDs. Maintaining a good correlation between the first and last sSD is an indicator of good performance in long-term extrapolation as the sSDs trained during periods separated by as many as 40-50 years were compared.

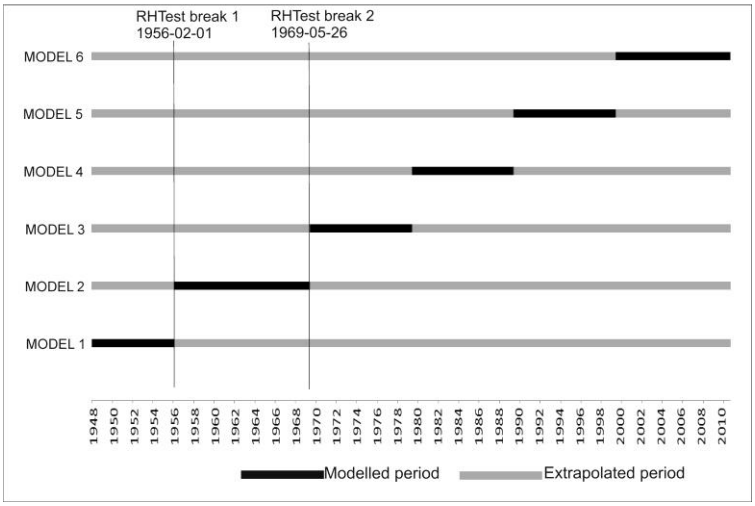

Figure 3: Division of the observed Tmin series of Alicante 'Ciudad Jardín' into stretches

To each stretch shown in black, sSD was applied, which was then extrapolated to the rest of the 1948-2011 period.

Tmax							**Tmax (HP filt.)**						
	SD 1	SD 2	SD 3	SD 4	SD 5	SD 6		SD 1	SD 2	SD 3	SD 4	SD 5	SD 6
SD 1	1.00	0.988	0.982	0.982	0.981	0.982	SD 1	1.00	0.951	0.926	0.923	0.917	0.924
SD 2		1.00	0.986	0.985	0.984	0.987	SD 2		1.00	0.944	0.937	0.930	0.944
SD 3			1.00	0.988	0.984	0.988	SD 3			1.00	0.950	0.932	0.951
SD 4				1.00	0.990	0.990	SD 4				1.00	0.956	0.959
SD 5					1.00	0.992	SD 5					1.00	0.965
SD 6						1.00	SD 6						1.00
Tmin							**Tmin (HP filt.)**						
SD 1	1.00	0.987	0.984	0.982	0.982	0.984	SD 1	1.00	0.932	0.918	0.908	0.900	0.914
SD 2		1.00	0.987	0.984	0.982	0.985	SD 2		1.00	0.932	0.920	0.905	0.924
SD 3			1.00	0.989	0.987	0.989	SD 3			1.00	0.946	0.932	0.944
SD 4				1.00	0.990	0.989	SD 4				1.00	0.941	0.946
SD 5					1.00	0.992	SD 5					1.00	0.959
SD 6						1.00	SD 6						1.00

Table 2: Correlation matrix ($\bar{x}$ all series) in the daily data among the sectorial SDs extrapolated to the whole 1948-2011 period. Left: raw data. Right: seasonal oscillation and low frequency cycles was removed by Hodrick-Prescott filtering. They were all statistically significant at 99.9% (student's t-distribution).

The differences in the long-term trends that gave sSDs of each series during the extrapolated period were assessed. No significant differences were found in their trends, particularly in the series that well fitted the sSDs to the observed data. Thus sSDs were coherent to each other during the extrapolated period in both short-term fluctuations and long-term trends.

The final SD per station was obtained from the weighted average of the SDs. Indeed the final SD was somewhat better than the sSDs when fitting the observed cross-validation data, and also during the training period of each particular SD. Hence in the final SD, this "multimodel" approach improved the estimation of the probabilistic range.

The final fit achieved by SD for the observed data was averaged with a mean absolute error (MAE) of 1.36ºC for Tmax and an MAE of 1.32ºC for Tmin in the daily data, and with MAEs of 0.26ºC and 0.23ºC for Tmax and Tmin, respectively, in the monthly data.

2.2. Reanalysis data

As a source of explanatory variables, the NCEP/NCAR reanalysis was taken (2.5ºx2.5º Lat/Lon grid) <http://nomad1.ncep.noaa.gov/cgi-bin/ftp2u_6p_r1.sh>. The variables used per grid point are described in Table 3. The data in the boundary layer (surface) were not employed because are more problematic according to a previous work (Rubinstein *et al*., 2004).

NCEP variable	Tmax ($\bar{x}$ 12h and 18h)		Tmin ($\bar{x}$ 00h and 06h)	
	Day 0	Day -1	Day 0	Day -1
TMP 1000 hPa	X	X	X	
TMP 925 hPa	X		X	
TMP 850 hPa	X		X	X
TMP 700 hPa	X		X	
HGT 1000hPa	X		X	
HGT 700 hPa	X		X	
U-GRD 1000hPa	X		X	

U-GRD 925hPa	X		X	
U-GRD 850 hPa	X		X	
U-GRD 700 hPa	X		X	
V-GRD 1000hPa	X		X	
V-GRD 925hPa	X		X	
V-GRD 850 hPa	X		X	
V-GRD 700 hPa	X		X	
RH 1000hPa	X		X	
RH 925hPa	X		X	
RH 850 hPa	X		X	
RH 700 hPa	X		X	
P-WAT	X		X	
4LFTX	X	X	X	X

Table 3: The reanalysis variables included as inputs in the SD done per grid point.

However for the SD done of each station, the variables that referred to the four closest grid points in the reanalysis were used. To this end, the original reanalysis grid points and an exact interpolation of the equidistant points to the original grid points were utilised. This is reflected in Figure 4, which depicts the boxes carried out for SD and the stations assigned to each box.

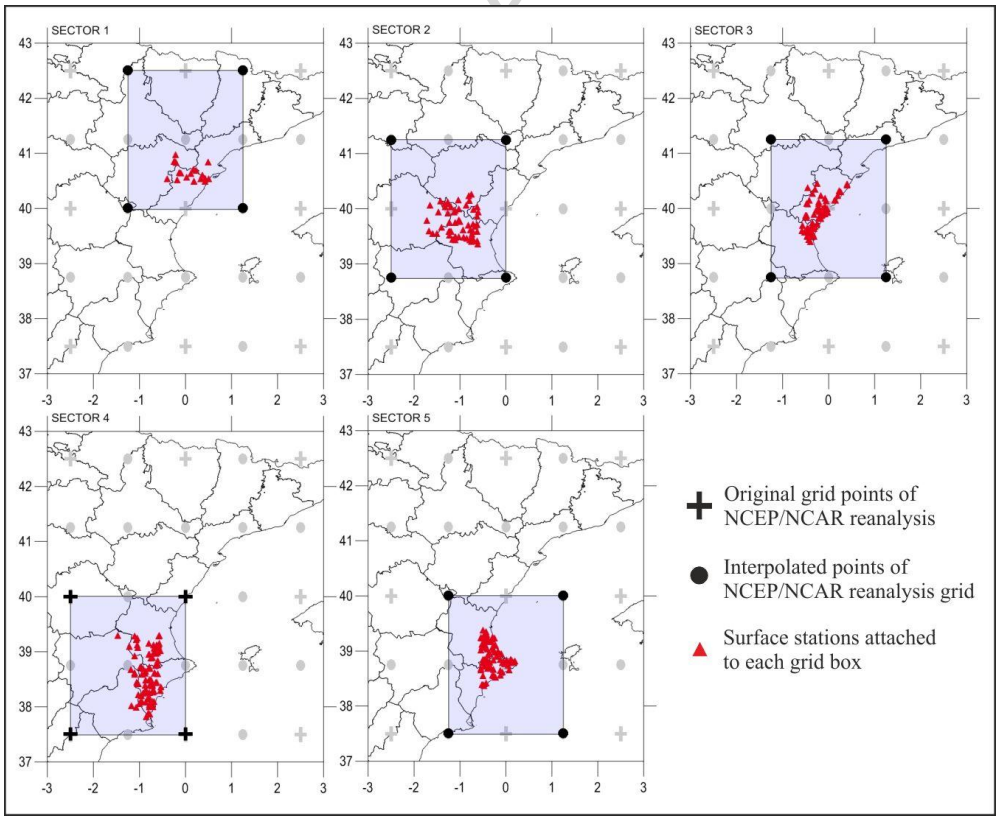

Figure 4: Grouping stations into five boxes of the four reanalysis grid points used to perform SD for each particular station.

Therefore for each SD, 88 variables were included (22x4), plus the seasonal oscillation of the solar constant; that is, 89 explanatory variables in all.

2.3. The SD technique

A hybrid artificial neural network (ANN) was employed. This ANN incorporated a modular cross between two types of weight layers (Figure 5). The first type (*the weight*

layer block) acts as a conventional ANN of the *multilayer perceptron* (MLP) type <http://www.peltarion.com/doc/index.php?title=Synapse:Weight_layer_block>. The second type is based on Hebb's learning (*the Hebbian layer block*) <http://www.peltarion.com/doc/index.php?title=Synapse:Hebbian_layer_block>. There were always eight neurons in each hidden layer.

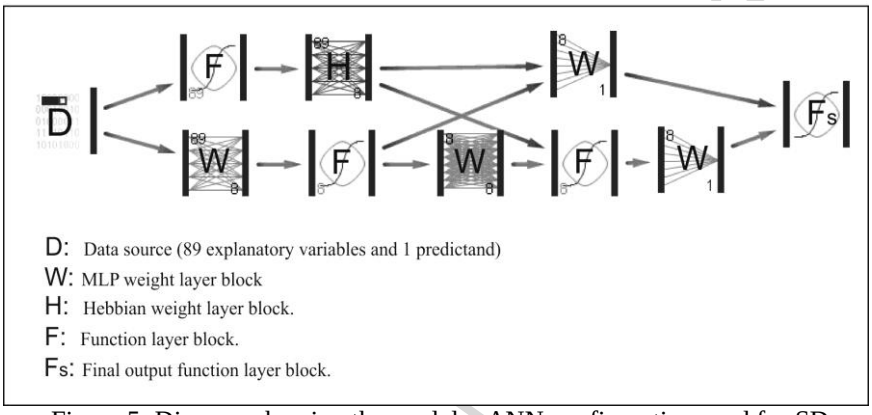

Figure 5: Diagram showing the modular ANN configuration used for SD.

The main reason for using a Hebbian ANN in parallel with MLP was the significant improvement gained in cross-validation, and there was much less overfitting with only one MLP-type ANN (the fit in the validation data became worse compared to the training data). It was not necessary to separate data seasonally or monthly to accomplish optimum ANN performance.

2.4. Trend and cluster analyses

Having obtained the final SD for all the series, the Mann-Kendall trend test was calculated for the annual SD series, and also for the 1948-2011 period, as was the Sen slope trend estimation method (Salmi *et al.*, 2002). The statistical significance of the trends at $\alpha = 0.001$, $\alpha = 0.01$, $\alpha = 0.05$ and $\alpha = 0.1$ was included for the Mann-Kendall test, and a 95% confidence interval was used for the Sen slope.

Having obtained the trends for all the series and for the whole 1948-2011 period, they were related with the group of physical factors characterising each station location type. These factors were:

a. Elevation.
b. Latitude.
c. Degree of continentality, measured (1 to 3) as distance from the coast: Less than 20km =1; between 20 and 40km = 2; more than 40km = 3.
d. Exposure to solar radiation, measured as the degree of terrain slope to the north or south, derived from a digital terrain model (DTM)
e. Potential nocturnal to air temperature inversion (0 to -3).

The last factor (e) refers to the distinct potentiality of accumulating cold night air owing to air temperatures inversion phenomena (the mountain-valley duo). This was calculated according to both the affluence-diffluence of the terrain by a laplacian operator and the absolute land slope, derived from the DTM. An example of this (the DTM derivative) is shown in Figure 6 (details of the Aitana zone).

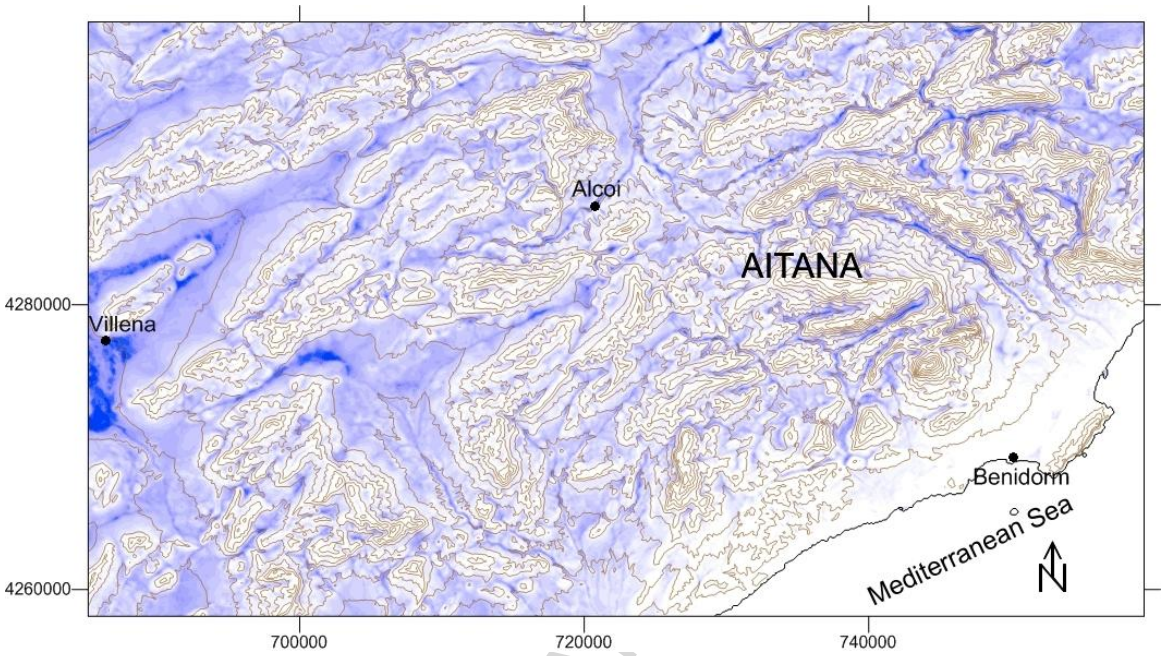

Figure 6: Example of the "potential nocturnal to air temperature inversion" DTM result (blue intensity). Elevation contours of 100 m are included.

In order to find relationships between thermal trends and the various location factors, a multiple correlation procedure was followed firstly by multiple linear regression. Secondly, a cluster analysis was done by Kohonen maps (Kohonen, 2001), known as SOM (Self-Organising Maps). This analysis, previously explained in Miró (2014) and Miró *et al*. (2014), revealed that the spatial distribution of some of these factors modulates air temperatures change trends on a local and regional scale, particularly for Tmin. Specifically, elevation and continentality were determinants for Tmax, and basically helped distinguish two clusters. However for Tmin, the topographical influence on the formation of night air temperatures inversion phenomena also played a key role as another more variable element in the local vicinity. Accordingly, five clusters or groups of series were differentiated, which displayed similar behaviour in the Tmin trends (Table 4). The multiple correlation results were consistent with clustering.

2.5. The SI technique

With the reconstructed series corresponding to the 1948-2011 period (the NCEP-NCAR reanalysis availability period), SI was done at a resolution of 90x90m over the whole study area and was carried out by ordinary kriging. The tests done using other interpolation techniques did not give better results than kriging did in the cross-validation, which denotes a sufficient station density for SI by kriging. Nevertheless, a blank mask was applied to the maps beyond the areas with the included stations because kriging did not give good results near the edges of the interpolated area.

The availability of derivative DTMs, e.g., exposure to solar radiation and the potential nocturnal to air temperature inversion, used initially for clustering stations, served to extrapolate the spatial modulation of air temperatures, which causes the relief, to the whole territory. This was done in accordance with what was observed in the stations, and not only due to height variation.

The gradient weights of these physico-geographical variables were estimated in accordance with the air temperatures available in the surrounding stations of each area by reduced major axis (RMA) regression. Several tests were done in distinct territorial

settings and in different months until the weighting in ºC of the original DTM values was found. This gave a better general result in cross-validation per month (Miró, 2014). This cross-validation was done by subtracting 40 stations, which were distributed aleatorily throughout the contemplated territory from one SI test (Figure 1). Yet some located in more difficult mountainous areas and in a lower station density were included on purpose. This entailed the risk that even a lower station density in these areas could make the SI validation result worse than the final SI employed.

Generally speaking, the fit accomplished in the cross-validation was better for Tmax than for Tmin. However the cross-validation result improved when the potential nocturnal to air temperature inversion DTM was incorporated into the SI for Tmin. Figure 7 shows the difference in the fit finally accomplished in the cross-validation for Tmin, when applying both the elevation DTM (only vertical gradient) and applying in addition the derivative DTM.

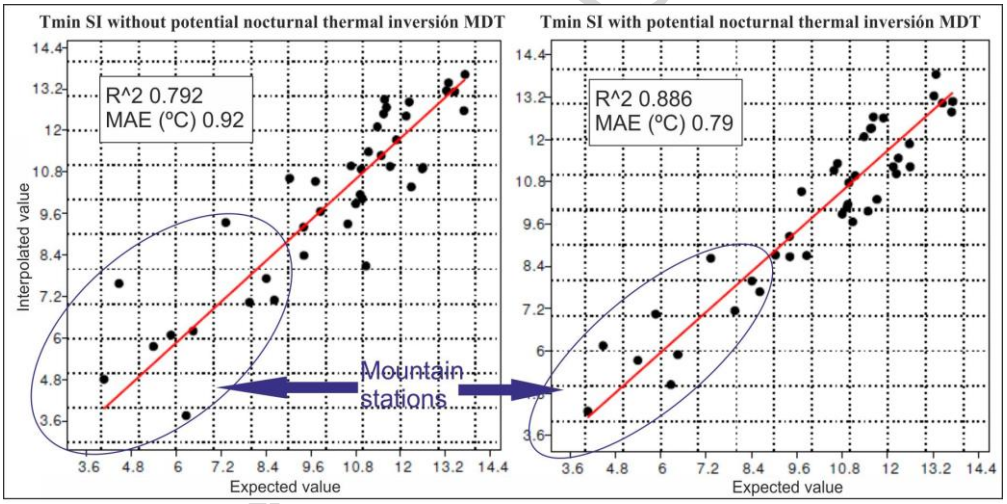

Figure 7: Cross-validation by RMA of the SI-interpolated Tmin values in relation to that expected in the control stations (1948-2011, average), by including, or not, the potential to the air temperatures inversion DTM. The coefficient of determination and mean absolute error (MAE) are shown.

For latitude and continentality, station density was estimated as being sufficient to reflect any variability in SI that depended on them. So no other DTM that explicitly expressed them was introduced.

The cross-validation results of the SI validation refer to the annual and monthly temperatures taken from the complete 1948-2011 period, (see Figure 8). Collectively, Tmin show a somewhat wider margin of error than Tmax (MAE of 0.36ºC for Tmax as opposed to 0.79ºC for Tmin for the yearly data).

SI allowed the modulation that the contemplated physico-geographical factors had on temperature, and therefore, on their air temperatures trends, to be covered over the entire analysed geographical space according to their weight, and also from the points where temperature information originally became available (stations).

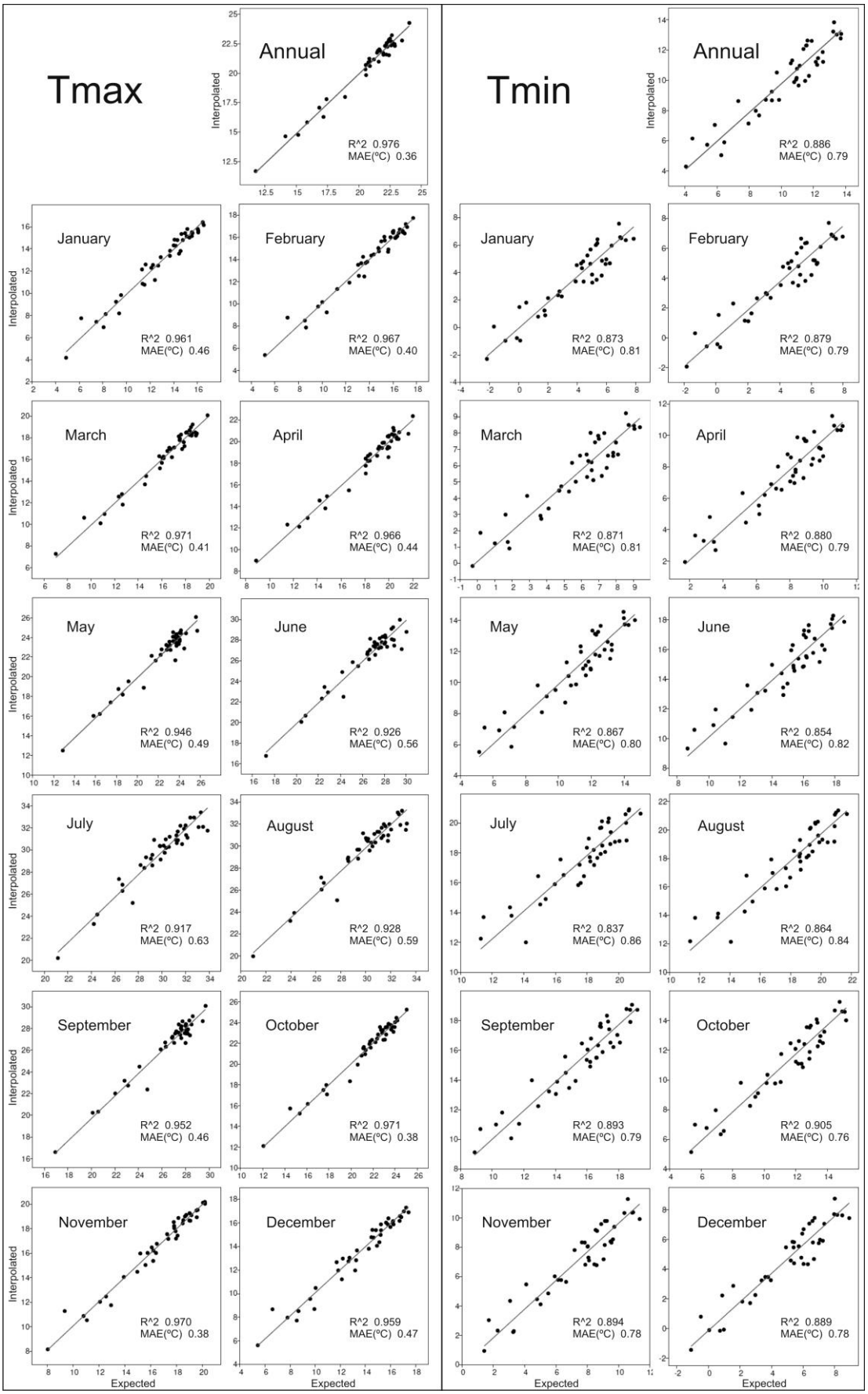

Figure 8: Cross-validation of SI by the linear regression (RMA) of the interpolated data in relation to that expected in the control stations. The coefficient of determination and mean absolute error (MAE) are included.

Nevertheless, trend testing was not feasible for all the 9,019,338 cells that were the object of interpolation, and which covered the whole analysed territory. As such testing has been previously done for the available SD series, the SI analysis was performed by calculating the magnitude of the air temperatures change that occurred between two periods: an initial one *vs.* a final one. For this purpose, a decadal analysis, like that done in Miró (2014) and Miró *et al*. (2014), was run. It established that within the 1948-2011 period, the greater increasing subperiod in air temperatures occurred between 1980 and 1998. Therefore a first subperiod between 1948 and 1979 was defined where, apart from typical cyclic climate oscillations, no long-term temperature trends took place. We took this finding as the baseline period. Hence from 1998, a pause, or a consolidation subperiod of change in air temperatures, was defined until 2011. We considered that calculating the magnitude of the average change during at least the last 15 years of the study period was a suitable measure (1997-2011) compared to the average baseline period (1948-1979).

2.6. Other variables used for potential climatic connections

To evaluate possible connections of the temperature trends results with other climate variables, have been used the following variables:

1. Wind speed and direction: Given the NCEP-NCAR reanalysis availability for the 1948-2011 period, we tested the tendency of wind derived for the U-GRD and V-GRD wind components from reanalysis. For this purpose, the two reanalysis grid points that coincided more with the Valencian Region coastline were used: 40ºN and 0ºW, and 37.5ºN and 0ºW. The average value of both points was taken at 1,000hPa. Their daily averages of prevailing wind direction and speed were taken (Miró, 2014). Were calculated the trends (Mann-Kendall trend and Sen slope) of the annual average of daily wind speed and annual frequency of days with winds per quadrant (mean or predominant in the four outputs per day of reanalysis). And finally were calculated the trends of the annual cumulative sum of the average daily wind speed, where the cumulative sum of the winds of the first and second quadrants are separated from those from the third and fourth quadrants.
2. Pressure: This was done by taking the daily averages from the NCEP-NCAR reanalysis (1948-2011), referred to as the reanalysis grid points in Table 4. The mean geopotential altitude (HGT) values at each grid point were calculated at 1,000hPa and 500hPa for the baseline (1948-1979) and the 1997-2011 periods by following the same temporal criterion to calculate magnitudes of air temperatures change by SI. Next the magnitude of change between both periods was calculated for each pressure level. The obtained data were interpolated, especially in the east Iberian Peninsula region (Miró, 2014).

Latitude	Longitude
42.5	-2.5
42.5	0
42.5	2.5
40	-2.5
40	0
40	2.5
37.5	-2.5
37.5	0
37.5	2.5

Table 4: The grid nodes in the NCEP/NCAR Reanalysis used in Figure 17.

3. Sea Surface Temperature (SST): in order to compare the SST tendencies in waters closer to the study area, we had to use satellite data (the NOAA/NASA database, 'AVHRR Oceans Pathfinder'). These data stem from the processing methods carried out by members of the meteorology and climatology team of the CEAM Foundation (Pastor et al., 2008; Pastor, 2012). This database covers only the 1985-2007 period, and from it, an average annual/monthly SST value was taken for the points over the sea between latitudes from 37.5ºN to 40ºN and longitudes from 1ºW to 2ºE. The series obtained in this way were submitted to the Mann-Kendall trend and Sen slope trend estimate tests

3. RESULTS

3.1. Air temperature trends of all the SD series grouped into clusters: determining factors

First of all, Table 5 presents the air temperatures trend results for each cluster and for the complete period (1948-2011). This table provides the values that indicate the physico-geographical factors, which were strongly related with air temperatures trends, as determined by the cluster analysis.

Physical-geographical factors (average values)	**Tmax**		**Tmin**				
	Cluster 0	**Cluster 1**	**Cluster 0**	**Cluster 1**	**Cluster 2**	**Cluster 3**	**Cluster 4**
Elevation (m).	**97.6**	**610.6**	**552.1**	**68.4**	**476.4**	**169.9**	**894.5**
Degree of continentality (1 to 3)[1]	**1.18**	**2.46**	**2.71**	**1.17**	**2.39**	**1.16**	**2.47**
Potential nocturnal to air temperature inversión (0 to -3)[2]	-	-	**-1.75**	**-1.62**	**-1.39**	**-0.53**	**-0.64**
MANN-KENDALL TEST(Z)							
ANNUAL	**3.86*** **	**4.43*** **	**-2.35***	-1.11	-0.41	0.68	**2.76****
JANUARY	0.96	1.64	-1.45	-1.22	-0.86	-0.52	0.54
FEBRUARY	0.69	1.25	**-1.91+**	-1.47	-1.08	-0.62	0.28
MARCH	1.47	**2.43***	**-2.44***	**-1.82+**	-1.25	-0.63	0.49
APRIL	**2.44***	**2.31***	-1.09	-0.54	-0.12	0.26	1.32
MAY	0.93	1.49	-0.68	-0.20	0.27	0.31	1.21
JUNE	**3.16****	**3.40*** **	0.65	0.86	**2.01***	**2.01***	**3.09****
JULY	**2.35***	**2.73****	0.10	0.64	1.18	1.20	**2.13***
AUGUST	**2.33***	**2.49***	1.48	**1.89+**	**2.00***	**2.32***	**2.42***
SEPTEMBER	-0.24	-0.78	-0.32	-0.13	-0.24	-0.05	-0.38
OCTOBER	**2.51***	**2.21***	0.45	1.09	1.21	**1.74+**	**2.29***
NOVEMBER	0.26	0.18	-0.81	-0.55	-0.18	0.06	0.02
DECEMBER	1.00	**1.77+**	**-2.11***	-1.48	-1.07	-0.81	0.01
SEN´S SLOPE IN ºC PER DECADE							
ANNUAL	**+0.12**	**+0.19**	-0.06	-0.03	-0.01	+0.02	**+0.09**
JANUARY	+0.10	+0.17	-0.13	-0.08	-0.05	-0.02	+0.04
FEBRUARY	+0.07	+0.17	**-0.19**	-0.13	-0.10	-0.05	+0.04
MARCH	+0.16	**+0.29**	**-0.21**	**-0.12**	-0.08	-0.03	+0.04
APRIL	**+0.18**	**+0.25**	-0.07	-0.03	-0.01	+0.01	+0.09
MAY	+0.07	+0.18	-0.03	-0.01	+0.02	+0.03	+0.10
JUNE	**+0.17**	**+0.35**	+0.03	+0.04	**+0.11**	**+0.10**	**+0.20**
JULY	**+0.13**	**+0.24**	+0.01	+0.04	+0.05	+0.06	**+0.13**
AUGUST	**+0.11**	**+0.19**	+0.07	**+0.09**	**+0.09**	**+0.09**	**+0.14**
SEPTEMBER	-0.02	-0.08	-0.02	-0.01	-0.02	+0.00	-0.02
OCTOBER	**+0.20**	**+0.23**	+0.04	+0.08	+0.09	+0.11	**+0.17**

NOVEMBER	+0.02	+0.02	-0.08	-0.05	-0.02	+0.01	+0.00
DECEMBER	+0.09	+0.15	**-0.18**	-0.12	-0.10	-0.07	+0.00

Table 5: Air temperature trends for the average of the series in each cluster. For the Mann-Kendall test, statistically significant trends are shown in bold as: *** ($\alpha = 0.001$), ** ($\alpha = 0.01$), * ($\alpha = 0.05$) + ($\alpha = 0.1$). The non-significant ones for any of the previous levels are depicted in grey. For Sen slopes, the exclusivity of the same sign slope within the 95% confidence range is denoted in bold. If the above condition is no longer satisfied, it is shown in grey. Clusters are ordered from the least to the most positive trends.[1] The most positive is greater. [2] The most negative is greater.

A clearly generalised increasing trend in air temperatures was observed for Tmax. However, the higher and inland sectors were those that showed a more marked trend (Cluster 1), which became more moderate the closer to the coast and pre-coastal depressions (Cluster 0). Conversely, more constrasts appeared with less significant trends for Tmin. The decoupling of these trends was caused by a clearly topographical factor (mountain-valley difference). Two antagonical clusters appeared and transition clusters were inserted between them, but they showed less clearly defined trends. The Tmin Cluster 0 presented less positive, and even negative, air temperature trends in continentalised settings, with a high potentiality to night air temperature inversion at a certain elevation, which resulted from its continentality; hence these are the stations located on plains or at bottoms of inland valleys. Conversely the latter, Cluster 4, presented the strongest increasing trends in air temperatures, which coincides with the stations located at higher elevation and with a low night inversion potentiality, but also with a slightly high degree of continentality. Here, therefore, the continentality factor played a reinforcing role of positive and negative trends. In fact Clusters 1 and 3 exhibited the same trend as their neighbouring clusters 0 and 4, be it somewhat weaker and not statistically significant at a less continental or coastal location. Cluster 2 included all the indefinite cases with no trend, and occupied a position of transition between bottoms of valleys and flat depressions, and also on mountain sides.

When disaggregating for months, the strongest and clearest positive trends appeared in summer and spring, especially in June, but also in October. The lull in September was very interesting as no trend occurred. The recorded negative trends were limited to winter months and to the first two Tmin clusters, when statistical significance was noted only for cluster 0. A tendency to more positive trends was generally maintained for Tmax, and the last Tmin clusters compared to the first ones, in most months. In many cases however, no statistical significance was obtained at the tested levels, and this was particularly true for winter months.

3.2. Evaluating the magnitude of air temperatures change and its spatial patterns with SI.

The air temperature change patterns observed in the trend analysis of the series are clearly seen in the SI maps, especially when compared with the relief in the area (Figure 1). However, it is now possible to establish the sectors in which extrapolation to the points with no available data estimates stronger change trends in air temperatures and their spatial distribution.

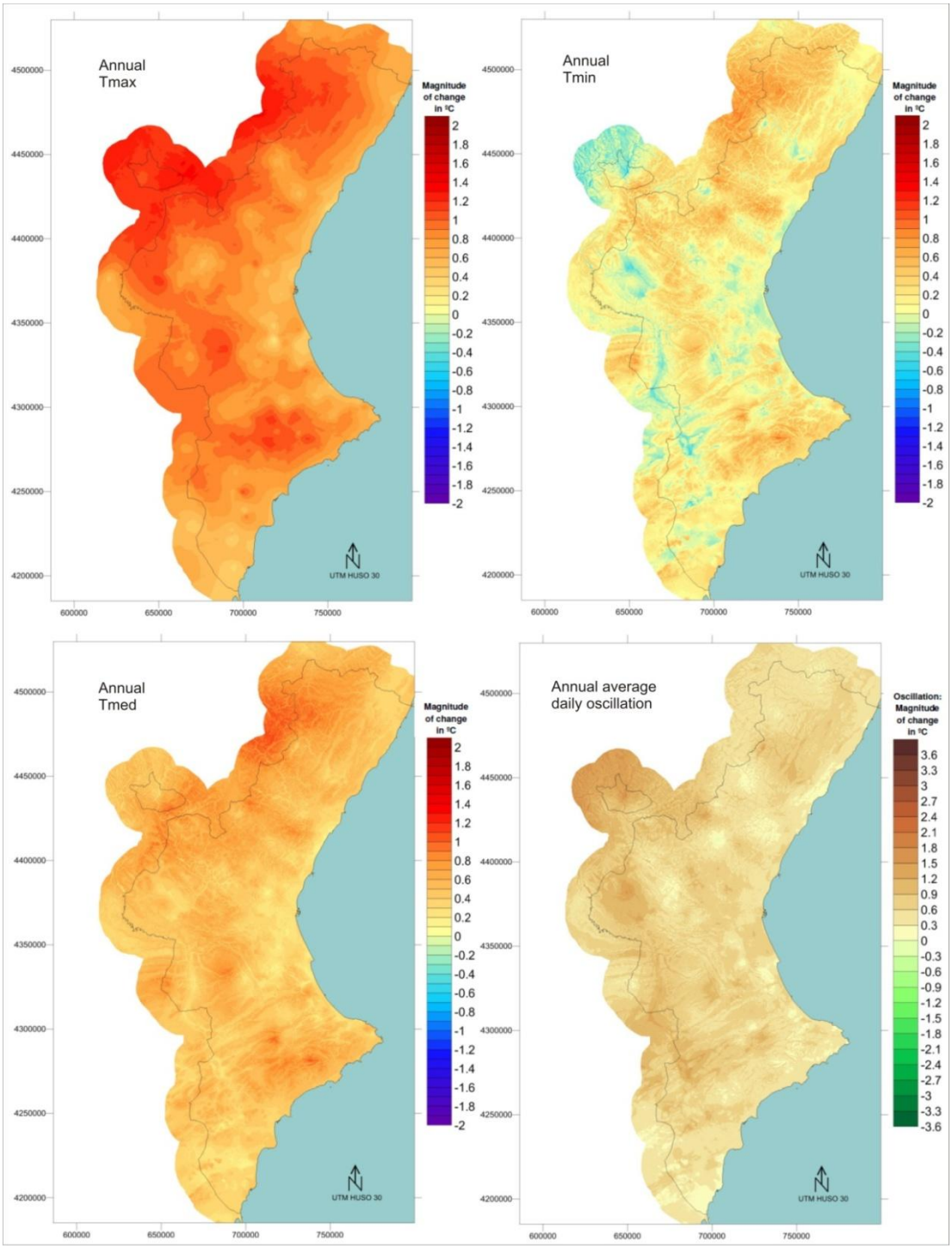

Figure 9: Magnitude of temperature change (°C) for the annual averages of Tmax, Tmin, Tmed and daily oscillation between the 1948-1979 period and the last 15 years of the series (1997-2011).

The annual results are offered first (Figure 9) and refer to the magnitude of the change calculated from the SI during the 1997-2011 period compared to the baseline period (1948-1979). Calculations for Tmax, Tmin, Tmed (average of Tmax and Tmin) are provided, along with the annual average of daily temperature oscillation (as the difference between Tmax and Tmin).

We can see that the highest warming rates exceed 1ºC (inland and high areas) for Tmax, and they reach 1.3ºC in the Iberian Mountain Range (the Gúdar and Javalambre Mountains). They also exceed 1ºC in the pre-Betico System of Alicante. The coastal

strip and precoastal depressions present a warming rate that does not generally exceed 0.7ºC (sporadically 0.5ºC). In contrast, we find more marked contrasts for Tmin and in the same spatial vicinity, with clear mountain-valley contrasts resulting from night air temperatures inversion phenomena. We also find that these contrasts are more marked inland and in mountainous areas than on the coastline. We observe warming rates (for Tmin) of 1ºC in the higher relief areas in the Iberian sector (Gúdar in particular), and also in culminations to the north of Alicante (the Aitana area), which run almost in parallel with Tmax. Conversely we find slight cooling rates that reach -0.6ºC in the bottoms of the valleys located in the more continental area of the Iberian sector, and also in depressions that lie more inland in the provinces of Valencia (center of region) and Alicante (south of region). These contrasts are reproduced more gently on the coastal strip, and slight warmings generally predominate, except in the precoastal depression of Valencia, with values that come close to 0. This means that generalised warming trends predominate for Tmed, but major geographical and spatial vicinity differences also exist. Thus the most marked magnitudes of change correspond to higher relief areas, and to a greater extent in the Gúdar Mountains (N, inland), but also to the peaks of the Aitana and Mariola Mountains (South), where temperatures exceed 1ºC. In contrast, weaker or more moderate warming was recorded in deeper areas in inland valleys, and on coastal plains and precoastal depressions (especially of Valencia), which barely reached 0.2ºC at some points.

A more pronounced increase for Tmax than for Tmin (particularly in more continentalised bottoms of valleys) spells a more generalised tendency to increased daily temperature oscillation. This could increase from 1.5º to 2ºC in the flatlands and valleys that lie more inland, and could remain below 0.5ºC on precoastal and coastal reliefs.

The results of the monthly air temperatures change in magnitude between the two indicated periods are presented below. Firstly the Tmax results are shown (Figure 10). June stands out as warming rose dramatically to 3ºC in the inland and high areas of the Gúdar and Javalambre Mountains (N, inland), and rose by between 2º and 3ºC in most of the study area. However, this warming appears to be milder in the precoastal plains and on the coastline because it did not generally go below 1ºC. The warming rates recorded from the second half of winter to August, and once again in October, are relevant. In October, no differences between the inland and coastal data were found, unlike the other months. We can state that summer temperature behaviour has clearly extended to June, and spring to March. In the second half of the year, the behaviour noted for September and November stands out because, on the one hand, it alternated with October and, on the other hand, it exhibited an almost opposite pattern to the rest of the year. Indeed these are the only two months when no generalised warming occurredor Tmax, and when slight negative anomalies appeared at points inland (preferably in the southern half), where significant warming occurred for the rest of the year.

Secondly, the Tmin results are provided (Figure 11). In this case, June was also the month with the largest magnitudes of warming, but constrasts were more marked. In high areas of Gúdar, SI estimated that warming could reach 2.3ºC, and could be even higher than 2ºC in pre-Betico System summits (southern half). This contrasts with the warming rates of 0.3ºC in the bottom lands of the precoastal depressions at center and south of region. In this case, October was also the month with more pronounced air temperatures increases, followed by other spring and summer months.

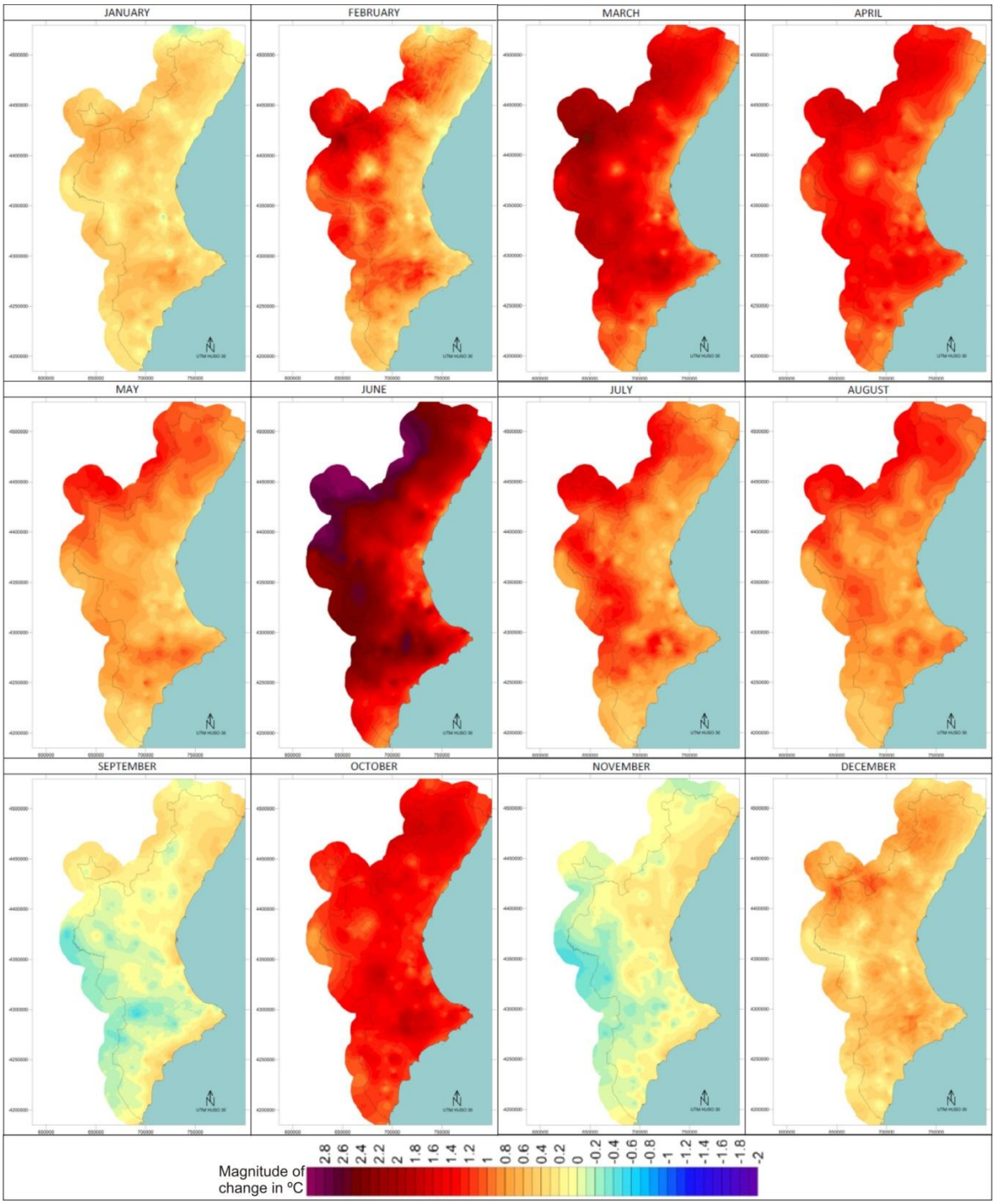

Figure 10: Magnitude of temperature change (°C) for the monthly averages of Tmax during the 1948-1979 period and the last 15 years of the series (1997-2011).

In winter months (December-February), negative anomalies appeared in all the sectors that were more affected by the air temperatures inversion phenomena associated with high pressures and wintry stability. These anomalies even went beyond -1.5ºC in more continentalised bottoms of valleys and bottom lands. Nevertheless in these winter months, warming trends remained outside valleys and depressions, especially in high areas of reliefs. March showed a transition to a greater predominance of positive anomalies, but strong contrasts remained in the spatial vicinity. It was only in September, and to a certain extent in November, that less marked spatial contrasts were

noted, with low magnitudes of warming or cooling. So once again, we observe a behaviour that is less connected to general trends.

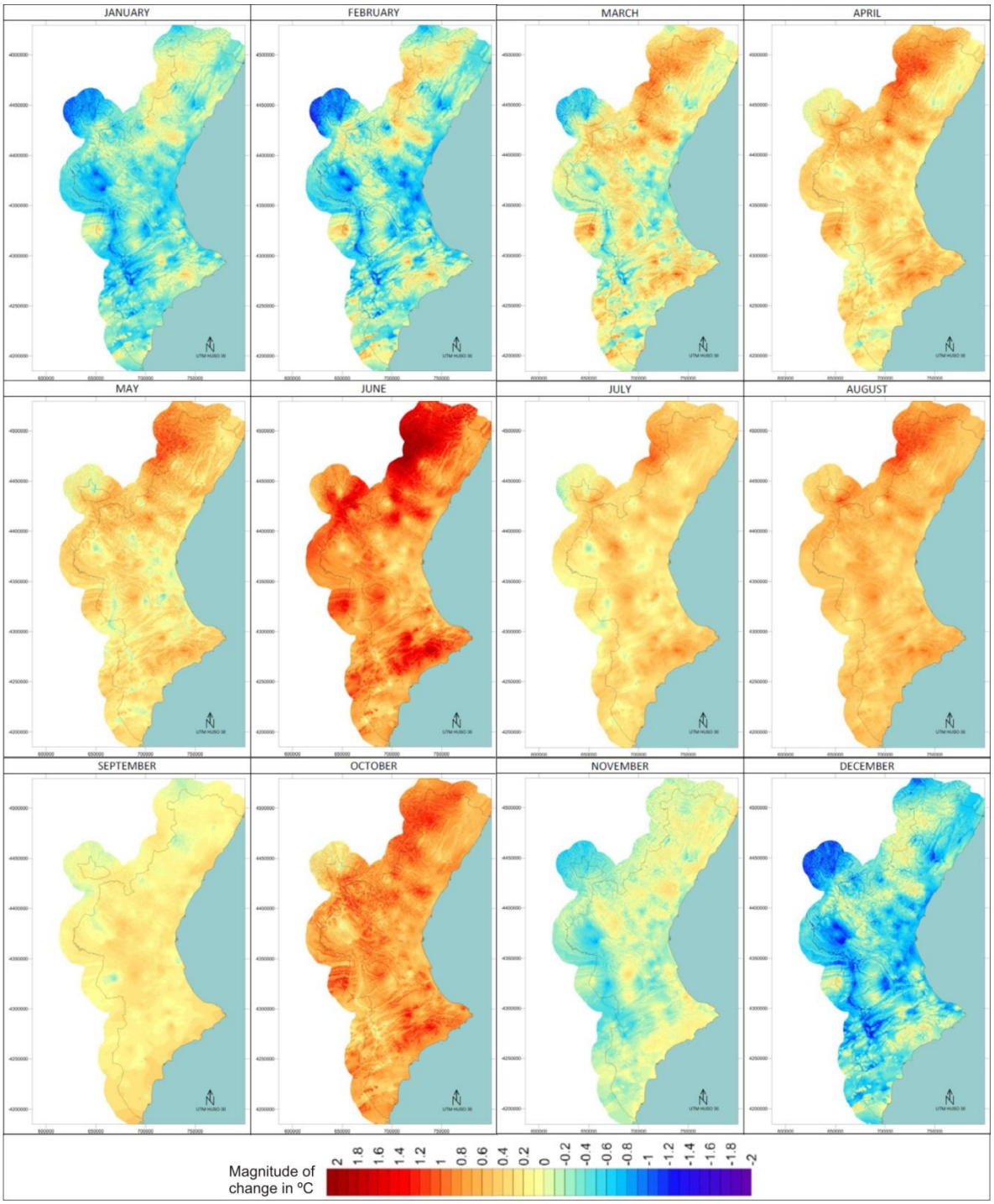

Figure 11: Magnitude of temperature change (°C) for the monthly averages of Tmin during the 1948-1979 period and the last 15 years of the series (1997-2011).

The previous results included the mean monthly temperature results, which are shown in Figure 12. Here we stress the result of warming for June, which reached up to 2.5ºC in higher parts of the Gúdar, Javalambre and Aitana mountains.

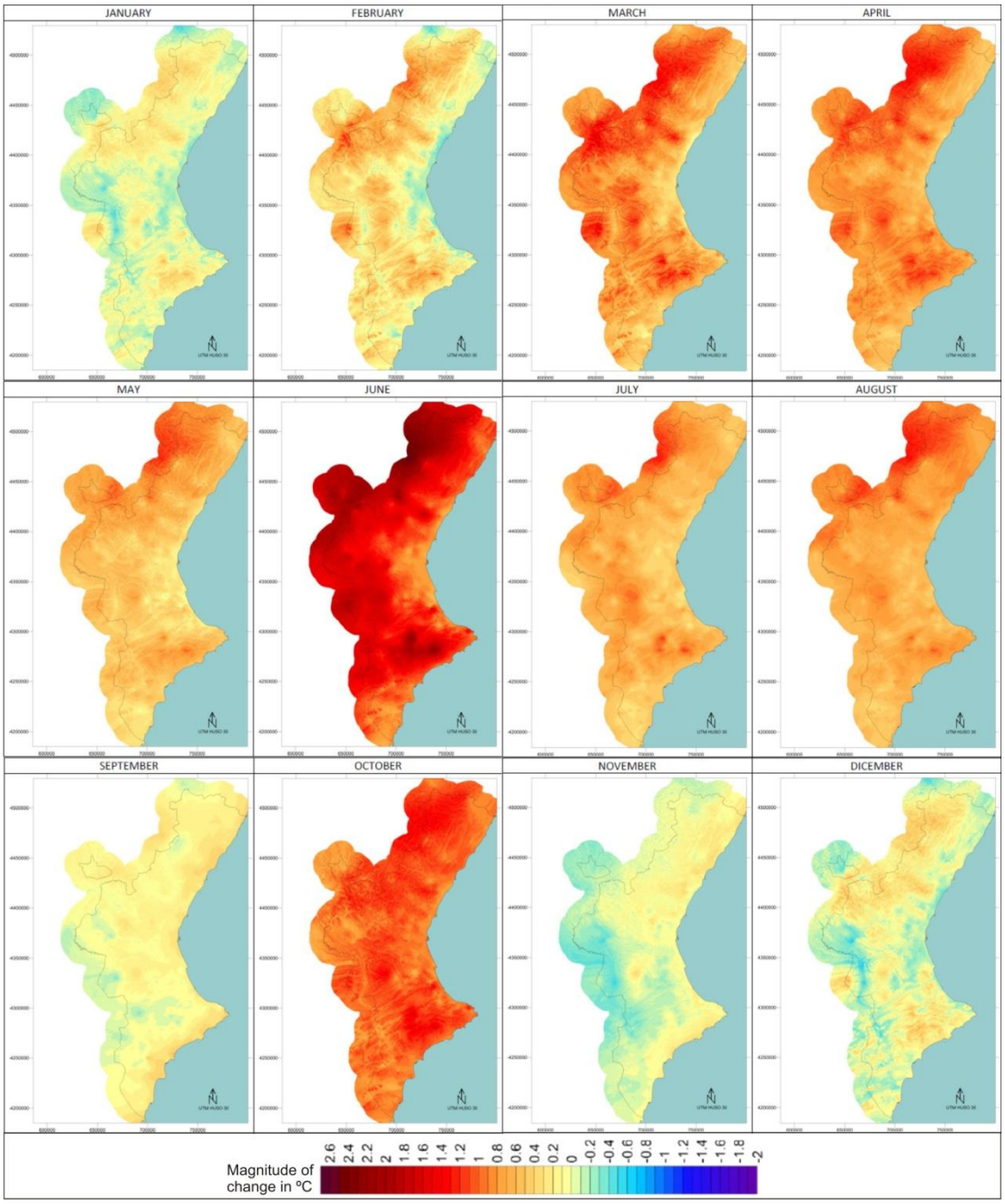

Figure 12: Magnitude of temperature change (°C) for the monthly averages of Tmed during the 1948-1979 period and the last 15 years of the series (1997-2011).

Finally, Figure 13 shows the changes in the monthly daily temperature oscillation averages. These results reveal that the daily thermal oscillations increased in most months, particularly those that showed a more pronounced pattern for mountain-valley decoupling in air temperature trends. In March, increases in temperature oscillation of up to 3ºC took place in the bottoms of the most inland valleys in the region. Conversely, September and November were not linked to these trends.

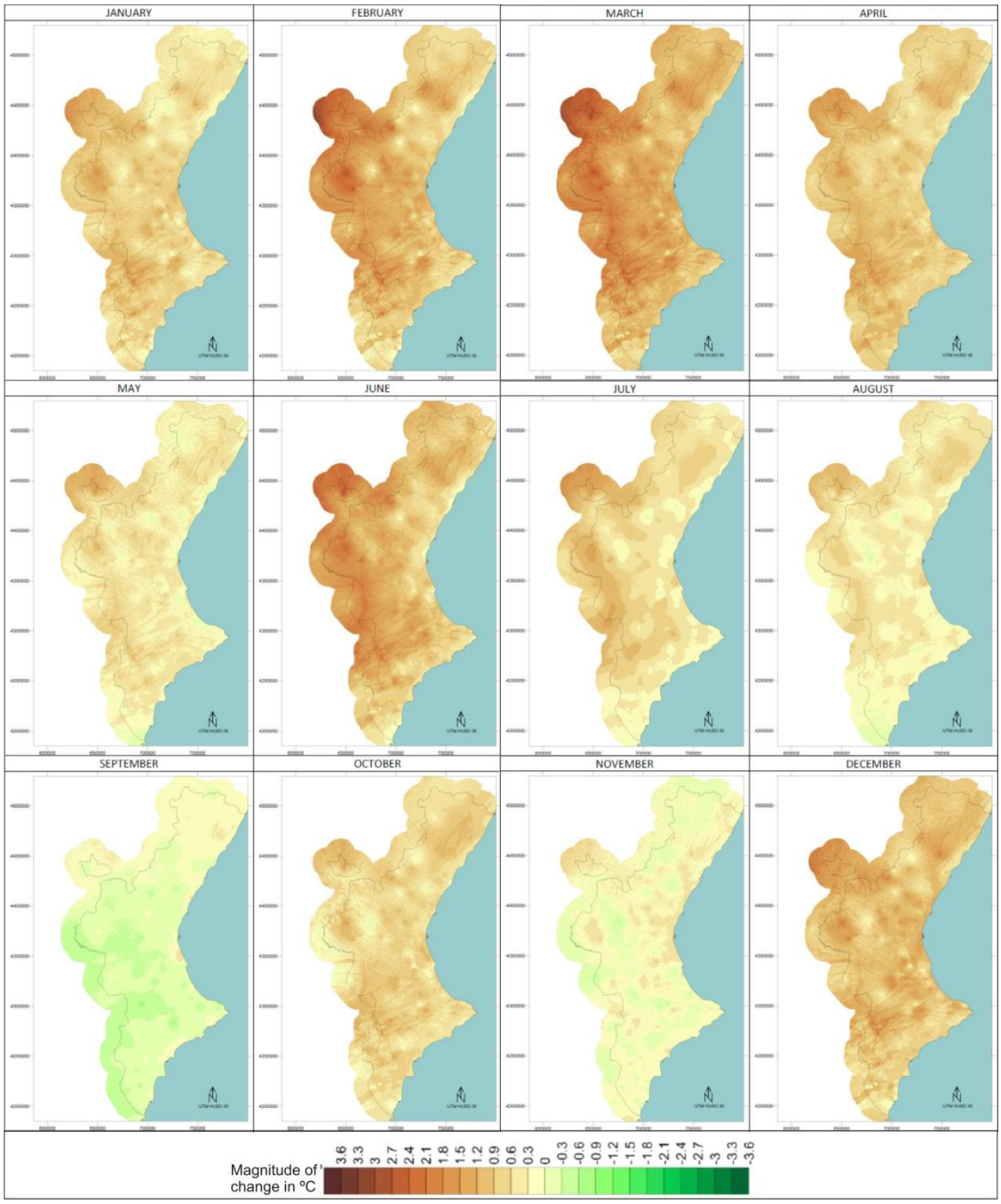

Figure 13: Magnitude of temperature change (°C) for the monthly averages of daily oscillation during the 1948-1979 period and the last 15 years of the series (1997-2011).

3.3. Climate connections of spatial change patterns

The fact that previous results are consistent with topographical and geographical factors seems to be related with possible changes in frequency of weather types, winds and pressure fields or circulatory patterns over the 1948-2011 period. For instance, the mountain-valley decoupling in air temperature trends apparently depends on more stable situations, or winds calming down, which produce higher temperatures in mountains, but air temperature inversion in valleys. The more moderate trends on the coast could also be related with a relative change in the frequency of sea winds *vs*. land winds, if compared to inland and high areas. The sea's soothing effect and the role of air temperature trends that sea surface temperature (SST) showed could also intervene.

First we can see (Figure 14) the tendency that the mean daily wind speed (provided annually) presents (1948-2011), along with the Mann-Kendall test and Sen slope estimation results. A significant downward trend is observed.

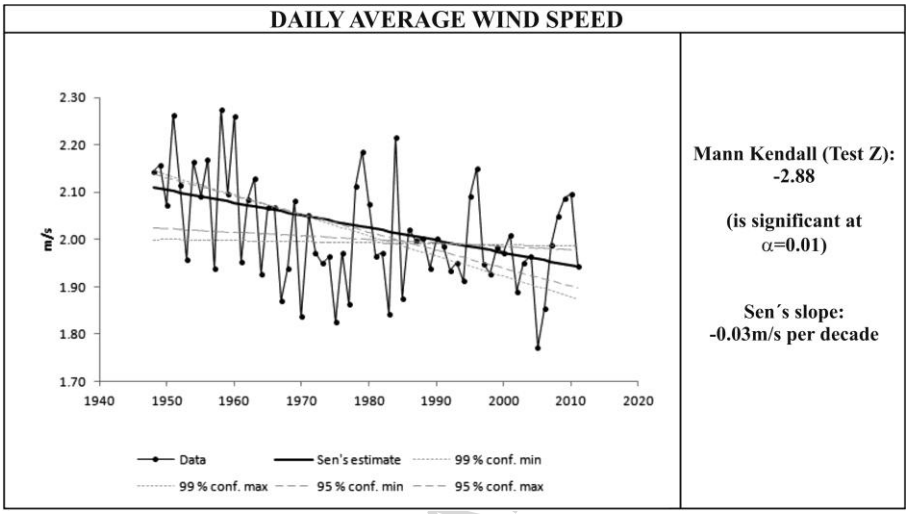

Figure 14: Trend for the annualised daily average wind speed (m/s) derived from the NCEP/NCAR for 40° N-0ºW and 37.5ºN-0ºW (1,000 hPa and the average for both points). Mann Kendall and Sen slope estimations are included along with their 95% and 99% confidence intervals.

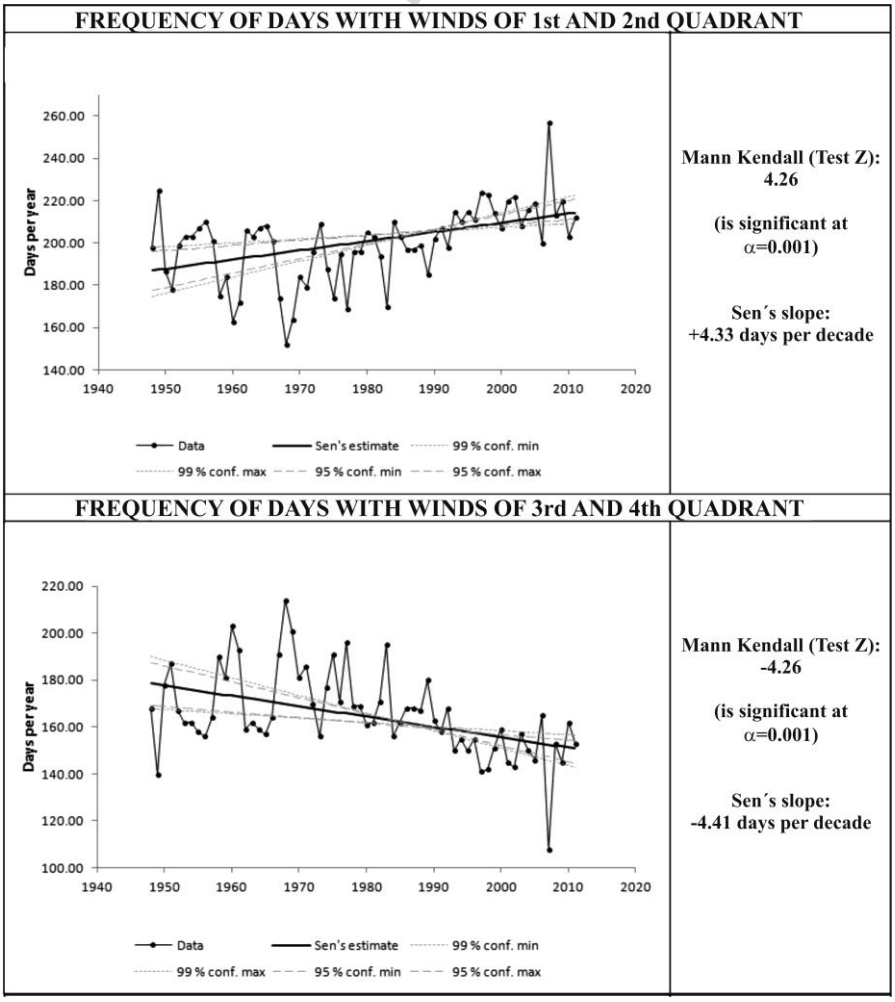

Figure 15: Trends for the number of days per year with winds from the first or second quadrants (top) or from the third or fourth quadrants (below). They derive from the NCEP/NCAR for 40° N-0ºW and

37.5ºN-0ºW (1,000 hPa and the average of both points). Mann Kendall and Sen slope estimations are included along with their 95% and 99% confidence intervals.

Then days of each year were grouped into two groups according to the predominant direction that the wind blew in: first- or second-quadrant winds (sea); third- and fourth-quadrant winds (land). Figure 15 shows the graphs that illustrate the annual frequency of land and sea winds, and the statistics of the trend between 1948 and 2011.

Figure 15 depicts a clear diversion in the frequency of land winds to sea winds. A significant upward tendency is seen for the first- and second-quadrant winds, while the trend is downward for the third- and fourth-quadrant one. Some 28 days a year moved from the first group to the second one throughout the study period.

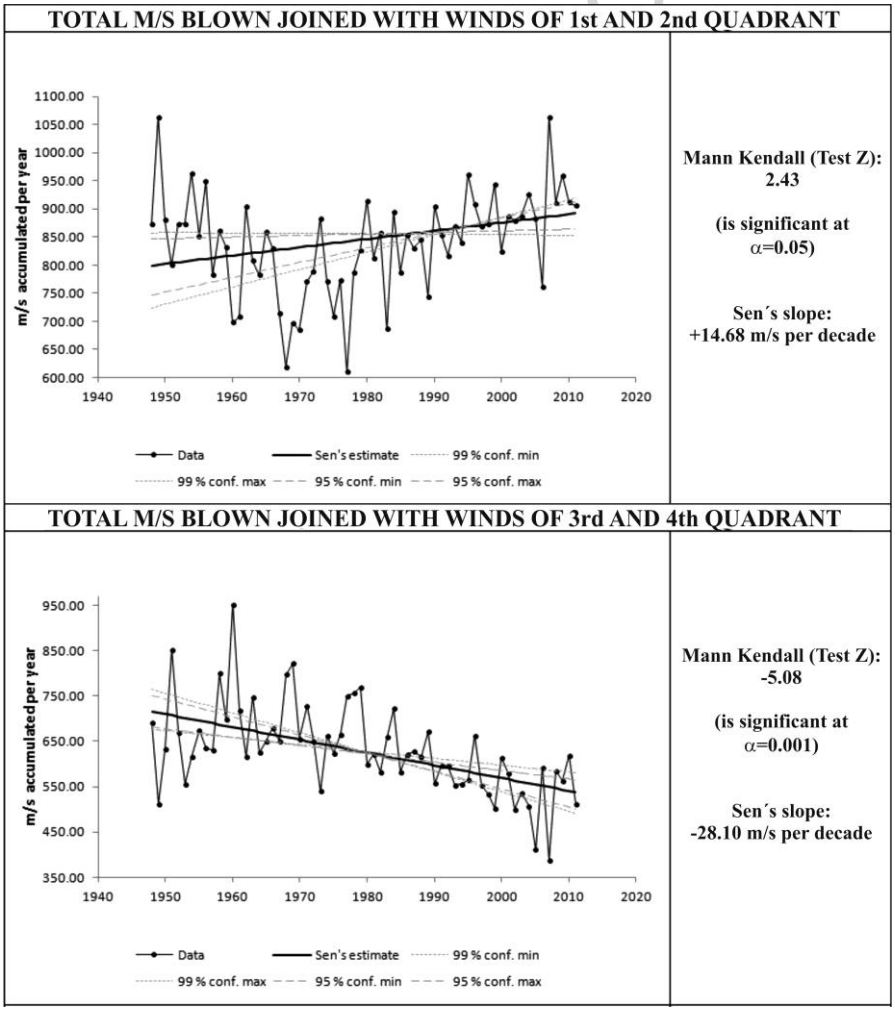

Figure 16: Trends for the annual cumulative sum of the average daily wind speed in m/s., where the cumulative sum of the winds of the first and second quadrants (top) are separated from those of the third and fourth quadrants (below). They derive from the NCEP/NCAR for 40° N-0ºW and 37.5ºN-0ºW (1,000 hPa and the average of both points). Mann Kendall and Sen slope estimations are included along with their 95% and 99% confidence intervals.

If we take the concept of comparing sea and land winds from a simple frequency to a total 'volume' of blown wind, which also implies speed, another reading stands out (Figure 16). The mean daily wind speed loss shown in Figure 14 is caused predominantly by a drastic loss in speed and weight for the land winds in the region, generally linked to westerlies associated with general atmospheric circulation in middle latitudes. Thus the strong downward tendency of the total annual 'm/s' blown by land

winds is not compensated by the moderate upward tendency of the total ‘m/s’ blown by sea winds. So we can state that the weight of the westerlies in the region diminished by almost one third throughout the study period (1948-2011).

To a great extent, these analysed wind-resulting elements already explain the behaviour of air temperature trends. Indeed, the more moderate warming trends on the coast can be linked to a reduced frequency of katabatic thermic trip phenomena that land winds provoke on the coast and in depressions. Reductions in mean wind speed can be related with more frequent situations of calm or breezes, which favour the formation of air temperatures inversion phenomena.

It is also interesting to compare possible changes in pressures fields as the causes of changes in wind frequency and speed, and also in stability-instability cycles. Figure 17 illustrates these results. It is worth comparing them with the results provided in figures 9 to 13. For annual values, the geopotential altitudes increased between both periods at both 1,000hPa and 500hPa; therefore, the frequency of high pressures also increased. However, the increase at 500hPa was greater, which suggests temperature warming forcing. This, in turn, determines a more pronounced tendency of stable conditions. The increase in HGT was also more pronounced north-westerly at 1,000hPa and north-easterly at 500hPa. This implis an increase in the first- and second-quadrant flows to the detriment of the third- and fourth-quadrant ones, and reasserts the scenario of more moderate air temperatute trends on the coast as opposed to a pronounced warming scenario inland and in elevated areas.

Winter months more markedly showed increases in the HGT at both 1,000hPa and 500hPa (December-March). March, and particularly February, presented the largest increase in atmospheric pressures, and a sharp rise in easterly or north-easterly flows (from the Mediterranean or inland Europe), which are associated with more stable situations. This suggest that mixed anticyclone situations in winter, which centred to Central Europe and to the northern Iberian Peninsula, notably increased, at least in February (but also in January). This explains the strong dissociation of air temperature trends between mountains and valleys given the increase in air temperature inversions, favoured by fewer gentle westerly winds. It also implies more irradiation phenomena and cold air accumulating in lower areas. However, higher parts are submitted to clear skies, more solar radiation and to cold air escaping to lower parts.

As from April and during the summer semester, the disparity between the changes occurring at 500hPa and those at 1,000hPa became wider. Whereas an upward change in pressure continued at 500hPa, the magnitudes of change at 1,000hPa tended to become smaller or more neutral. This can be associated with increasing low relative pressures on the surface of a thermic origin, which compensates part of the increase in high subtropical pressures at middle and high troposphere levels.

April, and particularly October, were the only months that presented increased land flows at both 1,000hPa and 500hPa. This explains why the differences in air temperature trends resulting from continentality in October were attentuated, unlike the whole annual set.

The marked increase in HGT at 500hPa in June is stressed, and is comparable to that recorded in winter months. Nonetheless, it showed a much less significant increase in HGT at 1,000hPa, and also in a lower baroclinic atmosphere. This suggests that stable situations, due to expanding high subtropical warm pressures, are dramatically increasing, and cause a clear weak thermic low manifestation on the surface level (almost 1,000hPa). Indeed this drives June towards typical summer behaviour, and explains why it is the month with the highest warming rate. The increased frequency of summer breezes, and a slightly increased frequency of easterly winds at 1,000hPa, could

also explain the more moderate warming scenario observed on the coastal strip compared with inland areas.

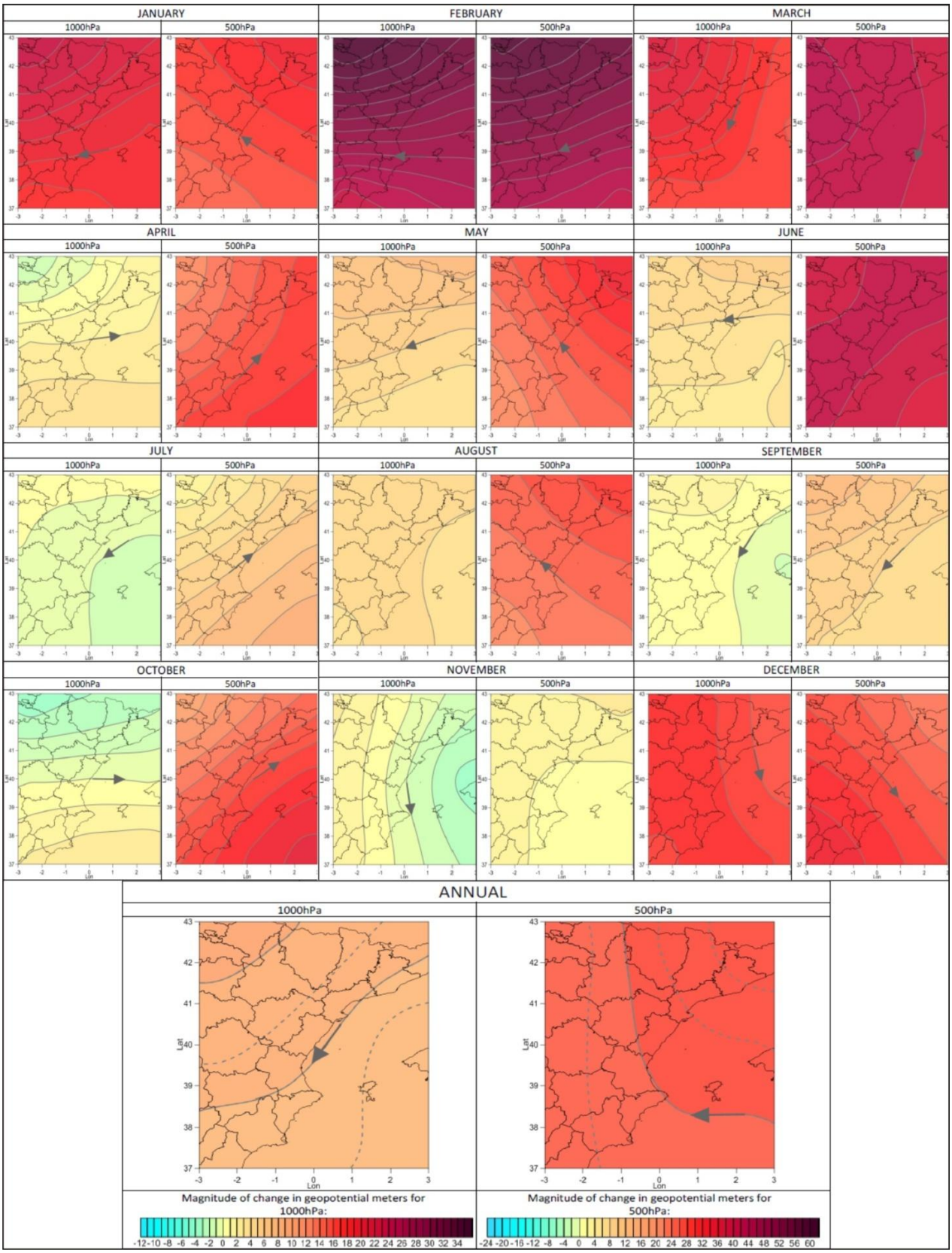

Figure 17: Change between the 1948-1979 and the 1997-2011 periods in the HGT (the mean of these periods) at the 1,000 hPa and 500 hPa levels, measured in geopotential metres of change. Calculations from the NCEP/NCAR, 2.5x2.5

September and November, which presented different air temperature change patterns to the rest of the year, also showed a distinct change pattern of pressures. These were the only two months in which the geopotential altitude at 500hPa barely increased according to the pattern of relatively lower pressures over the Mediterranean versus the northwest. This pattern became more marked at 1,000hPa, where the geopotential altitude lowered around the Balearic Isles, and where cyclone wind circulations increased. This suggests that the instability processes and mechanisms in autumn, which are typically Mediterranean, increased along with more frequent first-quadrant flows. To a great extent, this could explain the disconnection of the air temperature trends in these months from those of other months.

To some extent, July also showed a similar pattern of change to that of September, but at 1,000hPa and not at 500hPa. In any case, we can see that the increasing temperature changes in July were not so marked as in surrounding months of June and August.

Another element that supports the hypotheses of previous climate connections is precipitation. Several studies have focussed on this region and have reported a downward tendency of precipitations from the Atlantic, with a heavier weight towards inland areas. Conversely on the coast (especially the Gulf of Valencia), precipitations are maintained thanks to the increased relative weight of precipitations which originate in the Mediterranean (Estrela *et al*., 2004; Millán *et al*., 2005; Millán *et al*., 2006; Miró *et al*., 2006b; Miró *et al*., 2010; Estrela *et al*., 2010).

The final element to be verified was the role of the sea surface temperature (SST) close to the Valencia Region. However, the studies conducted on the Mediterranean SST that have dealt with changes in SST during our study period (1948-2011) are quite general throughout the Mediterranean, and have estimated an absolute warming rate of around 0.45ºC (Marullo *et al*., 2011). For the western Mediterranean basin, and over a shorter period, Skliris *et al.* (2012) estimated a warming slope of 0.22ºC per decade between 1973 and 2008 (the SST NOCS database, V.2, obtained *in situ*). This coincides with the mean air temperature increase in the land series on the coast deriving from SD (less than 20 km from the coast) for the same period.

In any case, in order to compare the SST tendencies in waters closer to the study area, we had to use satellite data described in 'Data and methods'(2.6). The trend results are shown in Table 6.

	Mann-Kendall (Z-Test)	**Sen slope in ºC/decade**	**Absolute magnitude of change between 1985 and 2007 (as in Sen slope) in ºC**
ANNUAL	**2.64****	**0.26**	**0.61**
JANUARY	0.85	0.16	0.36
FEBRUARY	1.27	0.17	0.39
MARCH	1.16	0.21	0.47
APRIL	**2.80****	**0.54**	**1.24**
MAY	**2.91****	**0.68**	**1.57**
JUNE	**2.64****	**0.68**	**1.57**
JULY	**1.90+**	0.40	0.92
AUGUST	0.63	0.11	0.25
SEPTEMBER	-0.85	-0.11	-0.26
OCTOBER	0.58	0.21	0.49
NOVEMBER	0.32	0.08	0.18
DECEMBER	0.42	0.07	0.16

Table 6: Trends for the SST average between latitudes 37.5ºN and 40°N and longitudes 1ºW to 2ºE for the 1985-2007 period according to the Mann-Kendall test and Sen slope estimations. For the Mann-

Kendall test, statistically significant trends are shown in bold as: *** (α = 0.001), ** (α = 0.01), * (α = 0.05) + (α = 0.1). Those that are non-significant for any of the previous levels are depicted in grey. For Sen slopes, the exclusivity of the same sign slope within the 95% confidence range is denoted in bold. If this condition is not met, it is shown in grey.

It is worth referring to Table 6 which, for the study period, coincides approximately with the period of most land temperature warming. For this reason, a comparison of trends should not be made absolutely, but relatively, as they are based on periods of different lengths.

We observe that the annual SST tended to increase, which occurred essentially in spring and summer months (April-July), whereas trends were not statistically significant at the testing levels for the rest of the year. When we ignored statistical significance, the more positive trend was noted in October compared to the surrounding months of September and November (which even became negative in September).

Therefore to a certain extent, the monthly SST trends also match not only the monthly land temperature trends in the region according to SD and SI, but also their connections with the atmospheric pressure change patterns.

All the former connections separately explain the obtained change patterns partially. Taken together, however, they provide a better explanation of these patterns.

4. DISCUSSION

The research done and the results obtained in Miró *et al*. (2012; 2014), Miró (2014) and in present study were considered an alternative solution in the analysis of local climate change patterns. Particularly when the spatial density of long series was insufficient, but density of shorter series is sufficient, a local signal sample is provided. However, the reconstruction and filling in of gaps in the temporarily inconsistent series observed by SD is debatable, which employs a signal from a reanalysis model because it could lack inhomogeneity. Likewise, the scientific literature recommends caution with SD products (Wilby et al., 2004; Hewitson *et al*. 2014). However numerous studies have indicated the validity of the signal deriving from global reanalysis models to study air temperature trends for mid-latitudes in the North hemisphere (Bengtsson *et al*., 2004; Rubinstein *et al*., 2004; Simmons *et al.*, 2004; CCSP, 2008), For instance, it has established a good correspondence in the study area between the NCEP-NCAR reanalysis and ERA-40, especially in winter despite higher dissimilarities in other regions of the globe (Sterl, 2004; Xue *et al.*, 2014). Furthermore, the use of a complex hybrid ANN, by modeling multiple sSDs cross-valitated, has allowed improve the SD error in respect to observed data. In this sense, the idea that hybrid or multi-model approaches tend to improve the performance of downscaling is reinforced (Tebaldi *et al.* 2007; Liu and Fan, 2014; Xue *et al.*, 2014). Nevertheless, perhaps the best way to determine an accurate temperature trend is to use relative homogenisation procedures with the observed series (Venema *et al*. 2012). Since availability of long series is scarce, the utilisation of only circular relative homogenisation among the observed series might not properly describe detailed differences on a local scale, provided mainly by the modulation that the relief and other physico-geographical factors can have on air temperature trends. This is because circular-type relative homogenisation tests can eliminate or amend the local variability components that are discordant with general behavior. So these tests are better for evaluating the general air temperature change signal of the group of series involved. This is the case when available scarce and short series, which are representative of the culminal mountain sectors in the area, are

homogenised with neighbouring reference series in valleys, and are submitted to different local processes; e.g., air temperature inversions and their frequency. This more local component can sporadically give rise to air temperature trends that differ from general ones, which is precisely the case in our study area; here different trends for minimum temperatures (Tmin) in nearby locations are strongly suggested in the present line of research to result from a distinct sensitivity to air temperature inversions caused by an increase in more favourable, stable situations. These increasing trends to the decoupling of Tmin in the mountain-valley tandem coincide with other results obtained at similar latitudes and in regions of complex terrain (Daly *et al*., 2010; Pepin *et al.*, 2011; Dobrowski *et al.,* 2011). Other recent results also suggest that a climate change in moisture conditions causes different responses in ground temperature trends, according to local topography factors or vegetation cover (Ashcroft and Gollan, 2013). Thus neighbouring observatories do not always share the same climate signal used as the baseline required for good relative homogenisation.

At this point, the SD followed in Miró *et al*. (2012; 2014) and Miró (2014), as a way to detect these different behaviours on a local scale, makes sense because, after all, it is a method used to indicate territory sectors that are potentially more vulnerable to climate change. It is also necessary to bear in mind that this SD was submitted to various validation processes used to minimise the problems usually associated with SD as much as possible. Therefore, the value of the results obtained and presented in this study does not merely reflect a global temperature change rate in the region (one that has, perhaps, been better estimated in other studies), but a novel revelation of local fine-scale change patterns in the territory. So it would be interesting to compare these results with others on a local scale using different procedures. Applying the methodology, but with other reanalysis models, e.g. the '20th Century NOAA Reanalysis, V2', would also be interesting.

Furthermore, the climate connections of the SD-SI results, herein related to possible changes in wind frequency and pressure patterns in the study area, support the results, and pose new questions and the need to better test these connections in future works. This applies to finding teleconnections among these patterns with decadal variability of major atmospheric circulation patterns; e.g., the North Atlantic Oscillation Index or the Western Mediterranean Oscillation Index. Regarding wind frequency, it is advisable to better validate the trends obtained with the re-analysis done with the surface wind data observed. Nevertheless, for these wind data, studies have indicated decreasing mean wind speed trends not only globally (e.g. McVicar *et al*., 2012), but also with the data observed in the Iberian Peninsula (Azorín Molina *et al*. 2014). This last work shows weak trends, but does not differentiate the origin of winds.

According to Vautard *et al.* (2010), stilling on the northern hemisphere mid-latitudes in the past 30 years may be partly attributed to a recent increase in vegetation and associated changes in roughness length (25-60%); increases of up to 50% may be attributed to atmospheric circulation changes, which seems to be the main cause herein.

Similar patterns of change to those shown herein are indicated when we look at future scenarios (A-2, IPCC) using high-resolution models that centre on the region; e.g. CGCM2, ECHAM4 and HadCM3 (Brunet *et al*., 2009), or CCSM and EH5 (Argüeso, 2012). A sharp increase in maximum temperatures, in daily temperature oscillations, which are stronger inland and in mountains than on the coast, plus more reduced precipitation inland than on the coast, have been observed in the aforementioned works, particularly in Argüeso (2012).

Finally, it is noteworthy that most former studies that have analysed general air temperature trends in the study area (Quereda *et al*., 2000; Miró *et al*., 2006a; Brunet *et*

al., 2007; Quereda *et al*., 2009; Bladé & Castro Díez, 2010; Del Río *et al.*, 2012) reflected on more positive trends for Tmin than the present study. Here it is essential to bear in mind that many stations in the region, particularly those on the coast, have had to withstand major urban development processes carried out in bordering areas. This circumstance has affected most of the available long series observed. Thus the doubt remains as to whether the relative homogeneisation processes in these studies, which are circular among the observed series, ended up including part of the predominant urban signal in the series so that Tmin would overweigh positive trends. Or if, conversely, if any inhomogeneity of the reanalysis or any change in climatic stationary relationships on which SD is sustained (e.g., forcing caused by climate change) would cause the positive trends in Tmin to be underweighted. Podría también ser el caso para las menor tendencia general al calentamiento encontrada en invierno con respecto al verano, ya que se han constatado para los meses invernales mayores If the latter were the case (or even a mixture of the former and latter), the value of the present study would be none the worse because it still indicates the most vulnerable areas to change in the territory, regardless of change being less pronounced or more pronounced.

5. CONCLUSIONS

The results of this work reveal that changes in the behaviour of temperatures have taken place in recent decades. They also show change patterns on a local and subregional scale, and differences depending on the time of year. These patterns may be related with relative changes in frequency of winds and advections in the pressure patterns of the region, and also with an increased frequency tendency of stable situations.

These change patterns firstly indicate a contrast between coast and precoastal depressions, with more moderate trends as opposed to higher and mountainous inland areas where more marked warming trends are seen. They also reveal a wider mean daily temperatures oscillation, which becomes more marked with continentality.

A stronger warming tendency is also indicated in spring and summer, especially in June, but also in October. This contrasts with the scarce tendencies seen in September and November, and with the marked air temperatures that decouple in the mountain-valley duo in winter months and for Tmin. The fact that this decoupling is detected for Tmin trends in the region is a novel aspect that is related with increased air temperature inversions. However, these findings fall in line with the results obtained in middle latitudes and complex reliefs in other world regions (Daly *et al*., 2010; Pepin *et al.*, 2011; Dobrowski *et al.*, 2011). Thus the obtained results back the hypothesis of a quicker change trend in higher mountain areas compared with valleys.

An assessment of these results and their connections with precipitation (Estrela *et al*., 2004; Millán *et al*., 2005; Millán *et al*., 2006; Miró *et al*., 2006b; Miró *et al*., 2010; Estrela *et al*., 2010) has evidenced that the sectors most exposed to climate change coincide with those that have a higher natural value, which shape the areas that recharge the aquifers and rivers supplying most human consumption in the region. When we consider that the SD and SI results did not contemplate a possible modification in the stationary relations that sustain them, the problem could become more serious if this change occurs with climate change.

ACKNOWLEDGEMENTS

This work has been made possible thanks to the Foundation 'Centro de Estudios Ambientales del Mediterráneo' (CEAM) located in Valencia, Spain, the University Institute 'Instituto Interuniversitario de Geografía' of the University of Alicante, the University Department 'Departamento de Geografía' of the University of Valencia and 'the Spanish Ministry of Economy and Competitiveness through Project no. CGL2011-30433-C02 (Termed). The English in this work has been proofread by Helen Warburton (a native English writer experienced in scientific works).

REFERENCES

Argüeso, D. 2011. *High-resolution projections of climate change over the Iberian Peninsula using a mesoscale model*. Ph. D. Thesis. Departamento de Física Aplicada. University of Granada.

Ashcroft, M. B., Gollan, J.R. 2013. Moisture, thermal inertia, and the spatial distributions of near-surface soil and air temperatures: Understanding factors that promote microrefugia. *Agricultural and Forest Meteorology* **176**(0): 77-89. DOI:10.1016/j.agrformet.2013.03.008.

Azorin-Molina, C., Vicente-Serrano, S.M., McVicar, T.R., Jerez, S., Sanchez-Lorenzo, A., López-Moreno, J.I., Revuelto, J., Trigo, R. M., Lopez-Bustins, J.A., y Espírito-Santo, F. 2014. Homogenization and assessment of observed near-surface wind speed trends over Spain and Portugal, 1961-2011. *Journal of Climate*, **27** (10), 3692-3712.

CCSP. 2008. *Reanalysis of Historical Climate Data for Key Atmospheric Features: Implications for Attribution of Causes of Observed Change. A Report by the U.S. Climate Change Science Program and the Subcommittee on Global Change Research*. National Oceanic and Atmospheric Administration, National Climatic Data Center, Asheville, NC, 156 p.

Bengtsson, L., Hagemann, S., Hodges, K.I. 2004. Can climate trends be calculated from reanalysis data?. *Journal of Geophysical Research*, **109**, D11111. DOI: 10.1029/2004JD004536.

Bladé, I., Castro-Díez, Y. 2010. Tendencias atmosféricas en la Península Ibérica durante el periodo instrumental en el contexto de la variabilidad natural. In: Pérez F, Boscoso R (eds.). *Clima en España: pasado,presente y futuro*, 25-42.

Brunet, M., et al. 2007. Temporal and spatial temperature variability and change over Spain during 1850–2005. *Journal of Geophysical Research: Atmospheres*, **112**, D12117. DOI: 10.1029/2006JD008249.

Brunet, M., Casado, M.J., De-Castro, M., Galán, P., López, J.A., Martín, J.M., Pastor, A., Petisco, E., Ramos, P., Ribalaygua, J., Rodríguez, E., Sanz, I., Torres, L. 2009. *Generación de escenarios climáticos regionalizados para España*. Agencia Estatal de Meteorología. Madrid, 157 p.

Daly, C., Conklin, D.R., Unsworth, M.H. 2010. Local atmospheric decoupling in complex topography alters climate change impacts. *International Journal of Climatology*, **30**, 1857–1864. DOI: 10.1002/joc.2007.

Del-Río, S., Cano-Ortiz, A., Herrero, L., Penas, A. 2012. Recent trends in mean maximum and minimum air temperatures over Spain (1921-2006). *Theoretical and Applied Climatology*, **109**, 605-626. DOI: 10.1007/s00704-012-0593-2.

Dobrowski, S.Z. 2011. A climatic basis for microrefugia: the influence of terrain on climate. *Global Change Biology*, **17**, 1022-1035.

Estrela, M.J., Miró, J.J., Pastor, F., Millán, M. 2004. Precipitaciones por frentes atlánticos en la Comunidad Valenciana: cambios y tendencias en las últimas décadas. *XXVIII Jornadas Científicas de la Asociación Meteorológica Española: La Meteorología y el Clima atlánticos*. Badajoz (Spain), 11-13 February 2004.

Estrela, M.J., Miró, J.J., Pastor, F., Millán, M. 2010. Frontal Atlantic rainfall component in the Western Mediterranean Basin. Variability and spatial distribution. ESF-MedCLIVAR Workshop on *Hydrological, socioeconomic and ecological impacts of the North Atlantic Oscillation in the Mediterranean region*. Zaragoza (Spain), 24-27 May 2010.

Hewitson, B.C., Crane, R.G. 1996. Climate downscaling: Techniques and application. *Climate Research*, **07**, 97-110.

Hewitson,B.C., Daron,J., Crane, R.G., Zermoglio, M.F, Jack, C. 2014. Interrogating empirical-statistical downscaling. *Climatic Change* **122:4**, 539-554.

Kohonen, T. 2001. *Self-Organizing Maps*. Third, extended edition. Springer, 501 p.

Liu, Y., Fan, K., 2014. An application of hybrid downscaling model to forecast summer precipitation at stations in China. *Atmospheric Research*, **143**, 17–30, DOI: 10.1016/j.atmosres.2014.01.024.

Maraun D., Wetterhall. F., Ireson, A.M. *et al*. 2010. Precipitation downscaling under climate change: recentdevelopments to bridge the gap between dynamical models and the end user. *Rev Geophys*, **48**, RG3003. DOI:10.1029/2009RG000314

Marullo, S., Artale, V., Santoleri, R. 2011. The SST Multidecadal Variability in the Atlantic–Mediterranean Region and Its Relation to AMO. *Journal of Climate*, **24**, 4385–4401. DOI: 10.1175/2011JCLI3884.1.

McVicar, T.R., Roderick, M.L., Donohue, R.J., Li, L.T., Van Niel, T.G., Thomas, A., Grieser, J., Jhajharia, D., Himri, Y., Mahowald, N.M., Mescherskaya, A.V., Kruger, A.C., Rehman, S., y Dinpashoh, Y. 2012. Global review and synthesis of trends in observed terrestrial near-surface wind speeds: Implications for evaporation. *Journal of Hydrology*, 416-417, pp.182-205.

Millán, M., Estrela, M.J., Miró, J.J. 2005. Rainfall components: variability and spatial distribution in a mediterranean area (Valencia Region). *Journal of Climate*, **18** (14), 2682-2705.

Millán, M., Estrela, M.J., Miró, J.J. 2006. Análisis de tendencias de la precipitación bajo situaciones de frente de retroceso en la Comunidad Valenciana (1959-2004). In: Cuadrat, J.M., et al. (Eds.). *Clima, Sociedad y Medio Ambiente*. Publicaciones de la Asociación Española de Climatología, A-5, 125-136.

Miró, J.J., Estrela, M.J., Millán, M. 2006a. Summer Temperature Trends in a Mediterranean Area (Valencia Region). *International Journal of Climatology*, **26**, 1051-1073.

Miró, J.J., Millán, M., Estrela, M.J. 2006b. Análisis de tendencias de la precipitación por frentes atlánticos en la Comunidad Valenciana (1959-2004). In: Cuadrat, J.M., et al. (Eds.). *Clima, Sociedad y Medio Ambiente*. Publicaciones de la Asociación Española de Climatología, A-5, 210-220.

Miró, J.J., Estrela, M.J., Pastor, F., Millán, M. 2010. Análisis comparativo de tendencias en la precipitación, por distintos inputs, entre los dominios hidrológicos del Segura y del Júcar (1958-2008). *Investigaciones Geográficas*, 49, 129-157. IUG. University of Alicante.

Miró, J.J., Estrela, M.J., Barberá, M.J. 2012. Análisis de tendencias de series diarias de temperatura a partir de un downscaling estadístico con datos de reanálisis y redes neuronales. Aplicación a la Comunidad Valenciana. In: Rodríguez-Puebla, et al. (Eds.). *Cambio climático. Extremos e impactos.* Publicaciones de la Asociación Española de Climatología, **A-8**, 549-560. <http://fundacion.usal.es/conaec/pendrive/ficheros/ponencias/ponencias2/30-Extremos.pdf>

Miró J.J. 2014. *Downscaling estadístico de series climáticas mediante redes neuronales: Reconstrucción en alta resolución de la temperatura diaria para la Comunidad Valenciana. Interpolación espacial y análisis de tendencias (1948-2011)*. Ph. D. Thesis. Instituto Interuniversitario de la University of Alicante, Fundación Centro de Estudios Ambientales del Mediterráneo, & Departamento de Geografía de la University of Valencia. 523p. <http://rua.ua.es/dspace/bitstream/10045/36538/1/tesis_juan_javier_miro_perez.pdf>

Miró J.J., Estrela, M.J., Olcina-Cantos, J. 2014. Reconstrucción de la señal térmica local en la Comunidad Valenciana entre 1948 y 2011 a partir de un downscaling estadístico mediante una red neuronal artificial: Detección de patrones locales de cambio. *Boletín de la Asociación de Geógrafos Españoles*. In Press, Accepted Manuscript.

Pastor, F.J., Estrela, M.J., Miró, J.J., Valiente, J.A. 2008. Meteorological Applications of the satellite-retrieved Sea Surface Temperature for the Forecast of Torrential Rains. In: Niclós, R. (Ed.). *Ocean Remote Sensing: Recent Techniques and Applications*, 133-144. Research Signpost.

Pastor, F.J. 2012. *Ciclogénesis intensas en la cuenca occidental del Mediterráneo y temperatura superficial del mar: Modelización y evaluación de las áreas de recarga*. Ph. D. Thesis. Departament d´Astronomia i Meteorologia. Facultat de Física. University of Barcelona. 199 p.

Pepin, N.C., Daly, C., Lundquist, J. 2011. The influence of surface versus free-air decoupling on temperature trend patterns in the western United States. *Journal of Geophysical Research*, **116**, D10109. DOI:10.1029/2010JD014769.

Pielke, Sr. R.A., Wilby, R.L. 2012. Regional climate downscaling: what's the point? Eos Forum, **93**, No. 5, 52-53 (Washington DC). DOI:10.1029/2012EO050008.

Quereda-Sala, J., Gil-Olcina, A., Pérez-Cueva, A., Olcina-Cantos, J., Rico-Amorós, A. Montón-Chiva, E. 2000. Climatic warming in the Spanish Mediterranean: natural trend or urban effect. *Climatic Change*, **46** (4), 473-483. DOI: 10.1023/A:1005688608044.

Quereda, J., Montón, E., Escrig, J. 2009. El cambio climático en las regiones de Valencia y Murcia: La sombra analítica de un auténtico troyano. *Investigaciones Geográficas*, **49**, 107-127. Instituto Universitario de Geografía. University of Alicante.

Rubinstein, K.G., Khan, V.M., Sterin, A.M. 2004. Qualitative comparison of air temperature trends based on ncar/ncep reanalysis, model simulations and aerological observations data» *35th COSPAR Scientific Assembly*. Held 18 - 25 July 2004, in Paris, France. p.2183.

Salmi, T., Määttä, A., Anttila, P., Ruoho-Airola, T., Amnell, T. 2002. *Detecting Trends of Annual Values of Atmospheric Pollutants by the Mann-Kendall Test and Sen's Slope Estimates – The Excel Template*

Application MAKESENS. Publication on Air Quality, Finnish Meteorological Institute, **31**, Helsinki, Finland.

Simmons, A.J., et al. 2004. Comparison of trends and low-frequency variability in CRU, ERA-40, and NCEP/NCAR analyses of surface air temperature». *Journal of Geophysical Research,* **109**, Issue D24. DOI:10.1029/2004JD005306.

Skliris, N., et al. 2012. Decadal scale variability of sea surface temperature in the Mediterranean Sea in relation to atmospheric variability. *Ocean Dynamics*, **62**, 13−30. DOI 10.1007/s10236-011-0493-5.

Sterl, A. 2004. On the (In)Homogeneity of Reanalysis Products. *Journal of Climate*, **17**, 3866–3873. DOI: 10.1175/1520-0442(2004)017<3866:OTIORP>2.0.CO;2.

Tebaldi, C., Knutti, R. 2007. The use of the multi-model ensemble in probabilistic climate projections. *Philosophical transactions. Series A, Mathematical, physical, and engineering sciences*, **365**(1857), 2053-2075. DOI: 10.1098/rsta.2007.2076.

Vautard, R., Cattiaux, J., Yiou, P., Thépaut, J.-N., y Ciais, P. 2010. Northern Hemisphere atmospheric stilling partly attributed to an increase in surface roughness. *Nature Geoscience*, **3** (11), 756-761.

Venema, V.K.C., et al. 2012. Benchmarking homogenization algorithms for monthly data. *Climate of the Past*, **8**, 89-115. DOI:10.5194/cp-8-89-2012.

Wilby, R.L., et al. 1998. Statistical downscaling of general circulation model output: A comparison of methods. *Water Resources Research*, **34** (11), 2995–3008. DOI:10.1029/98WR02577.

Wilby, R.L., Charles, S.P., Zorita, E., Timbal, B., Whetton, P., Mearns, L.O. 2004. *Guidelines for use of climate scenarios developed from statistical downscaling methods*. Supporting Material of the Intergovernmental Panel on Climate Change. 27 p.

Xue, Y., Jajnic, Z., Dudhia, J., Vasic, R., De Sales, F. (invited). 2014. A review on regional dynamical downscaling in intra-seasonal to seasonal simulation/prediction and major factors that affect downscaling ability. *Atmospheric Research. Volumes*, **147-148**, 68-85. DOI:10.1016/j.atmosres.2014.05.001.

HIGHLIGHTS

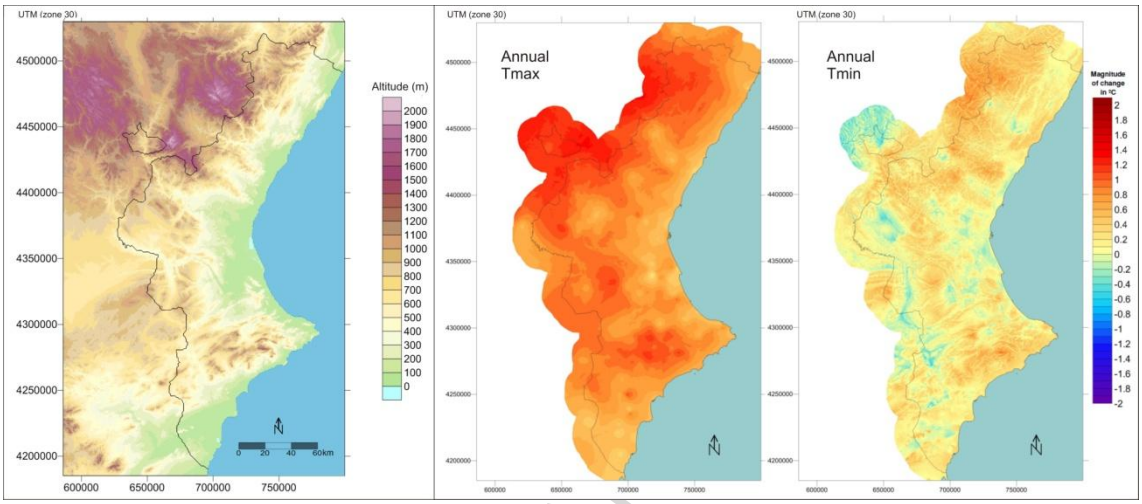

Magnitude of temperature change (°C) for the annual averages of maximum (center) and minimum (right) temperatures, between the 1948-1979 period and the last 15 years of analyzed series (1997-2011). It is based on a statistical downscaling for reconstruct a large number of incomplete observed series in the Valencia region for the NCEP-NCAR Reanalysis availability period (since 1948) and 90x90 m spatial interpolation. Sub-regional and local climate change patterns are revealed. Relief is included (left) for reference.

Graphical abstract